Microbubble-assisted ultrasound for imaging and therapy of melanoma skin cancer: A systematic review

François Avry, Coralie Mousset, Edward Oujagir, Ayache Bouakaz, Valérie Gouilleux-Gruart, Rose-Anne Thépault, Sylvaine Renault, Sylviane Marouillat, Laurent Machet, Jean-Michel Escoffre

Microbubble-assisted ultrasound for imaging and therapy of melanoma skin cancer: A systematic review

François Avry[1], Coralie Mousset[1,2], Edward Oujagir[1], Ayache Bouakaz[1], Valérie Gouilleux-Gruart[2], Rose-Anne Thépault[1,3], Sylvaine Renault[1], Sylviane Marouillat[1], Laurent Machet[1,4], Jean-Michel Escoffre[1*]

[1]*UMR 1253, iBrain, Université de Tours, Inserm, Tours, France*

[2]*GICC EA 7501, Université de Tours, Tours, France.*

[3]*Present address: UMR 1307, CRCI2NA, Université de Nantes, Inserm, Nantes, France*

[4]*Department of Dermatology, Tours University Hospital, Tours, France*

To whom correspondence should be addressed: J-M. Escoffre, PhD., Inserm UMR 1253, Université de Tours, 10 bd Tonnellé, 37044 Tours Cedex, France. Tel. +33 (0) 247366191. Email: jean-michel.escoffre@univ-tours.fr.

Abstract

Recent technological developments in ultrasound (US) imaging and ultrasound contrast agents (UCAs) have improved the diagnostic confidence in echography. In the clinical management of melanoma, contrast-enhanced ultrasound (CEUS) imaging complements conventional US imaging (*i.e.,* high-resolution US and Doppler imaging) for clinical examination and therapeutic follow-up. These developments have set into motion the combined use of ultrasound and UCAs as a new modality for drug delivery. This modality, called sonoporation, has emerged as a noninvasive, targeted, and safe method for the delivery of therapeutic drugs into melanoma. This review focuses on the results and prospects of using US and UCAs as dual modalities for CEUS imaging and melanoma treatment.

Keywords: Melanoma, ultrasound, microbubble, imaging, drug delivery, therapy.

INTRODUCTION

Despite recent improvements in prevention, diagnosis, and treatment, malignant melanoma (MM) is the most aggressive and deadliest skin malignancy, with an increasing incidence in Europe (Ferlay, et al. 2018). The estimated incidence rates in Europe were 15.8/100 000 men and 14.6/100 000 women in 2018. Although MM is less common than other skin cancers, it is more lethal. In 2018, approximately 27 100 deaths were caused by MM in Europe (Ferlay, et al. 2018). When MM is diagnosed at an early stage (*i.e.,* localized stage or stages I–II), it can be efficiently treated. Indeed, MM is curable with surgery at this stage, with a 5-year specific survival rate of 98% (Dowling, et al. 2019). Patients with more advanced disease or in metastatic stages have worse outcomes. Conventional treatments, including chemotherapy and radiotherapy, are ineffective, with a 5-year survival of 5% (Dowling, et al. 2019). Nevertheless, new expensive biological drugs (*i.e.,* immunotherapy with checkpoint inhibitors) or targeted therapy (BRAF and MEK inhibitors) have been designed in recent years, which may prolong survival with a specific 5-year survival of 50% (Sarkisian, et al. 2020). Currently, the average cost of diagnosis and treatment of MM is 10 times greater than that of nonmelanoma skin cancer (Karimkhani, et al. 2017). The productivity loss due to morbidity and premature mortality also contributes to a socioeconomic burden on society (Karimkhani, et al. 2017). In this context, biomedical research is ongoing to develop innovative methods for the early diagnosis and treatment of this aggressive skin cancer to reduce its morbidity and mortality while minimizing its socioeconomic burden.

Detection and staging of skin melanoma are critical with regard to treatment and patient outcomes. Later diagnosis significantly increases the risk of metastatic disease. The gold standard for the diagnosis of MM is based on the histological examination of the total removal of the lesion (Ramalingam and Allamaneni 2020). The pathology report must include Breslow thickness (using the ocular micrometer), ulceration, presence of microsatellites, mitotic rate,

and margin to perform an accurate staging of melanoma. Breslow thickness, also called the Breslow index, is considered the main prognostic factor for metastatic potential. This index determines the margin sizes of surgical resection of the primary lesion and the probability of microscopic involvement of regional lymph nodes that can be identified using the sentinel lymph node biopsy (SLNB) procedure (Bichakjian, et al. 2011). While radionuclide lymphoscintigraphy provides a roadmap for surgeons (Tardelli, et al. 2016), single-photon emission computed tomography/computed tomography (SPECT/CT) imaging provides a more accurate 3D visualization of SLNs than lymphoscintigraphy (Chapman, et al. 2016). SPECT/CT helps in planning the surgical procedure by providing valuable anatomical and functional information concerning the tissue and vascular structures surrounding the SLNs. If the presence of metastases in SLNs is confirmed, 1-year adjuvant treatment with immunotherapy or BRAF/MEK inhibitors may be proposed. ^{18}F-fluorodeoxyglucose positron emission tomography/computer tomography (^{18}F-FDG PET/CT) imaging is currently used to detect suspicious distant melanoma metastases in clinical stage IIc disease (Schroer-Gunther, et al. 2012). Both whole-body ^{18}F-FDG PET/CT and dynamic contrast-enhanced magnetic resonance imaging (DCE-MRI) are recommended to assess the location and extent of brain metastases in stage III and higher disease. Finally, elevated blood lactate dehydrogenase levels are associated with poor outcomes and are utilized for stratification at advanced stages in the American Joint Committee on Cancer 8th edition (Gershenwald and Scolyer 2018).

More recently, ultrasound (US) imaging has been proposed as a real-time, non-ionizing, and low-cost imaging modality for melanoma diagnosis (Cammarota, et al. 1998). In B-mode, the melanoma appears as well-delimited, fusiform, homogeneous, and hypoechoic lesions on high-resolution US imaging (7–20 MHz) compared with other lesions (Corvino, et al. 2017). This modality provided thickness measurements that were well correlated with histological Breslow thickness measurements for lesions larger than 1 mm in thickness (Serrone, et al. 2002). The

use of very high-frequency probes, *i.e.,* > 20 MHz, is strongly recommended for the accurate measurement of lesions less than 1 mm in thickness (Gambichler, et al. 2007). In addition, US imaging of draining LNs at low frequency, *i.e.,* 5–10 MHz, is recommended when physical examination presents contradictory findings (Catalano 2011). US examination of regional LNs is advised before SLNB for a broader exploration of LNs in the body regions related to metastatic disease (Voit, et al. 2010). Moreover, an appropriate US imaging-guided preoperative mapping of the tumor lesion and the detection of melanoma infiltration in relevant anatomic structures (*e.g.,* fascia, muscles, and bone cortex) allows improving surgical management, including the best surgical approach and the choice of appropriate surgical margins with low surgical risk, while enhancing the cosmetic prognosis of the patient (Chaput, et al. 2018, Machet, et al. 2009). In addition, Doppler imaging has revealed that primary cutaneous melanoma frequently appears hypervascular (Lassau, et al. 2002, Lassau, et al. 2006). The vascular density was positively correlated with Breslow's tumor thickness (Lassau, et al. 2002). Both vascular density and Breslow's tumor thickness are significantly correlated with metastatic dissemination (Lassau, et al. 2006).

However, the introduction of ultrasound contrast agents (UCAs) in the late 1990s revolutionized the evaluation of tumor microvasculature by providing more accurate and sensitive information than color/power Doppler imaging. These agents are used to enhance specific body compartments and tissues (Frinking, et al. 2020). Thus, contrast-enhanced ultrasound imaging (CEUS) has become a complementary imaging modality to conventional US imaging for the clinical examination and therapeutic follow-up of patients with melanoma. In addition, the combined use of US and UCAs as a new modality for drug delivery in the treatment of melanoma has been under investigation for a few years. In this review, we focus on the combined use of US and UCAs as a dual modality for CEUS imaging and melanoma treatment. The limitations of the available literature and future perspectives are discussed.

METHODS

PubMed® and Web of Science™ electronic databases were screened by two authors of this review (FA and JME) using predefined search dates (January 1995–December 2021) and terms for *in vivo* and clinical studies investigating the contributions of microbubble-assisted ultrasound for the management of melanoma. The PubMed® database search terms used were: (melanoma [MeSH terms] OR melanoma skin cancer [MeSH terms]) AND (microbubbles [MeSH terms] OR ultrasound contrast agents [MeSH terms]) AND (ultrasound [MeSH terms] AND Sonoporation [MeSH terms] AND microbubble-assisted ultrasound [MeSH terms] AND dynamic contrast-enhanced ultrasound) AND ("English" [language]). The research terms ("melanoma OR melanoma skin cancer") AND ("microbubbles OR ultrasound contrast agents") OR ("ultrasound" OR "microbubble-assisted ultrasound") were used on the Web of Science™. The research term "ultrasound AND melanoma" was used in both databases. The inclusion and exclusion criteria are summarized in **Table 1**. All *in vivo* and clinical procedures mentioned in this review were performed according to ethical guidelines and approved by the Animal Care and Regional Committee for Ethics in Animal Experimentation. Data were extracted by the same authors by following a pre-defined list, including melanoma, melanoma skin cancer, ultrasound parameters (frequency, duty cycle (DC), total insonation time, pulse repetition frequency (PRF), and peak negative pressure (PNP)), and microbubble characteristics (type, dose, and administration route). The selection schedule is shown in **Figure 1**. Sixty-seven publications met our inclusion criteria (**Table 1**).

CONTRAST-ENHANCED ULTRASOUND IMAGING (CEUS)

Principle

Ultrasound contrast agents (UCAs) are used to enhance specific body compartments and tissues (Frinking, et al. 2020). This relative enhancement provides key anatomical, morphological, functional, and molecular information, which is essential for prognosis, diagnosis, lesion

characterization, and therapeutic follow-up. UCAs are aqueous solutions of gas microbubbles (MBs) (Sennoga, et al. 2017). Perifluorinated gases are preferred for UCAs. These gas MBs are surrounded by a biocompatible shell, which prevents coalescence and reduces gas dissolution in the blood. A large majority of commercially available MBs are stabilized by a phospholipid monolayer that is more acoustically effective because of its thin (*i.e.,* 2–3 nm) and highly elastic shell than polymer MBs. Their size is in the 2–5 μm range (Frinking, et al. 2020). Thus, after intravenous (i.v.) injection, these MBs are confined to the entire vasculature, including the smallest capillaries, making them pure intravascular tracers. The half-life of UCAs after i.v. injection is typically few minutes (Sennoga, et al. 2017). This duration is sufficient for imaging purposes and has the added advantage that several consecutive injections or infusions of UCAs can be achieved safely (Frinking, et al. 2020). Because of their compressibility, MBs exposed to US undergo nonlinear volumetric oscillations at a high mechanical index (MI) (Frinking, et al. 2000). In this nonlinear oscillation mode, the nonlinear signal components of echo signals backscattered by the MBs are specific to MBs and are not present at a significant magnitude in tissue echoes (Frinking, et al. 2000). Several imaging modes (*e.g.,* second harmonic imaging, pulse inversion, and power modulation) have been developed to preferentially capture these nonlinear components while reducing echoes from nonperfused tissues (Averkiou, et al. 2020). These new advances have considerably improved the sensitivity of UCA detection, allowing real-time two-dimensional and three-dimensional (3D) imaging. Recent advances in image and signal processing methods (*e.g.,* deconvolution and skeletonization methods) have allowed for an accurate description and characterization of the tumor microvascular network (Gauthier, et al. 2012, Molinari, et al. 2014). These methods provide reliable quantitative parameters for assessing tumor perfusion for diagnostic and therapeutic follow-up purposes.

Moreover, ultrasound molecular imaging relies on the i.v. injection of targeted MBs that bind specific overexpressed endothelial biomarkers of angiogenesis (*i.e.,* endoglin, vascular

endothelial growth factor receptor-2) and adhesion (*i.e.,* $\alpha_v\beta_3$ integrin) processes, which play a major role in tumor progression (Klibanov 2020). These MBs are functionalized by attaching a targeting agent (*i.e.,* ligand, full, or fragment of antibody or peptide). After their i.v. injection, a fraction of targeted MBs binds the endothelial biomarkers, whereas several of them freely circulate into the blood stream because of the speed of blood flow. The acoustic signal from adherent MBs can be differentiated into circulating MBs using dedicated CEUS modes (Leguerney, et al. 2015). Thus, US imaging assesses the expression levels of target endothelial biomarkers to identify and quantify changes in angiogenesis and adhesion processes involved in melanoma progression.

Diagnosis and characterization of primary melanoma

The performance of CEUS in the diagnosis and characterization of primary melanoma has mainly been assessed in a mouse melanoma model (**Figure 2; Table 2**). As expected, Schroeder *et al.,* reported that Doppler imaging is not as sensitive as CEUS for detecting melanoma neovascularity in a syngeneic mouse melanoma model (Schroeder, et al. 2001). The correlation between the percentage of vessel area and the histologic grade of vascularization was significantly improved when CEUS was used. In addition, Gauthier *et al.,* demonstrated that CEUS can provide seven semiquantitative (*i.e.,* peak intensity, slope to wash-in, time to peak intensity, full width at half maximum, area under the curve, area under the wash-out, and area under the wash-in) and three quantitative perfusion parameters (*i.e.,* blood flow, blood volume, and mean transit time) with low intraoperator variability to quantitatively assess the perfusion of melanoma (Gauthier, et al. 2011, Gauthier, et al. 2012). Among these perfusion parameters, Pitre-Champagnat *et al.,* reported that the area under the curve and the peak intensity are significantly correlated to the microvessel density but not to the diameter and maturity of blood vessels (Pitre-Champagnat, et al. 2015). These preclinical investigations demonstrated that

CEUS provides reliable perfusion parameters for characterizing the microvasculature of primary melanomas.

Moreover, Forsberg *et al.,* described that CEUS measures of tumor neovascularization provide a noninvasive biomarker of neoangiogenesis, corresponding to the expression of molecular biomarkers of neoangiogenesis (*e.g.,* cyclooxygenase-2 and vascular endothelial growth factor (VEGF)) in both human melanoma xenograft models (Forsberg, et al. 2002, Forsberg, et al. 2008). In this context, *in-vitro* and preclinical studies have reported the design and validation of $\alpha_V\beta_3$ integrin-, endoglin-, and VEGF receptor 2 (VEGFR2)-targeted UCAs in the US molecular imaging of melanoma neovascularization (Leguerney, et al. 2015). These biomarkers are overexpressed at the surface of the melanoma microvasculature, and their expression is positively correlated with tumor grade. Thus, Leguerney *et al.,* investigated the expression levels of endoglin, $\alpha_V\beta_3$ integrin, and VEGFR2 using US molecular imaging in murine melanoma models (Leguerney, et al. 2015). To achieve this goal, the microvasculature and expression levels of these endothelial biomarkers were assessed using UCAs conjugated with dedicated and biotinylated monoclonal antibodies. The results revealed that endoglin is more highly expressed on the surface of melanoma microvasculature than $\alpha_V\beta_3$ integrin and VEGFR2, suggesting that US molecular imaging using endoglin-targeted UCAs may be used for the noninvasive longitudinal evaluation of tumor angiogenesis during melanoma growth (**Figure 3**). In addition, the authors also demonstrated that the efficacy of anti-angiogenic treatments, *e.g.,* sorafenib, on tumor angiogenesis can be detected by assessing the downregulation of endoglin expression at the surface of the tumor microvasculature (Leguerney, et al. 2015).

All of these studies show that the clinical potential of CEUS as well as molecular US imaging are complementary modalities for the detection and characterization of melanoma, as well as for the prediction of the efficacy of antiangiogenic treatment. Unfortunately, these studies were

mainly conducted on animal models of melanoma. Further clinical investigations should be performed to confirm these preclinical studies and determine the performance of this imaging modality in a clinical context.

CEUS of advanced stages

In this subsection, we discuss the performance of dynamic contrast-enhanced ultrasound (DCEUS) in the diagnosis of melanoma metastases in the lymph nodes, liver, and gallbladder because their presence in other organs is preferentially detected and characterized using PET-CT imaging and/or MRI (**Table 2**) (Dinnes, et al. 2019).

Lymph nodes

SLNB is the current standard procedure for detecting and identifying metastases in LNs. However, Bertelsen *et al.,* identified three main limitations of this method (Bertelsen, et al. 2019): 1) the radiotracer detects secondary LNs, resulting in their dissections, thereby increasing operative time and morbidity; 2) if the primary lesion is located near the draining nodal basins in areas with a dense lymphatic supply, the use of a hand-held gamma probe is more challenging; and 3) lymphoscintigraphy does not offer depth information for anatomic SLN localization. To overcome this issue, the surgeon removes LNs and assesses them *ex-vivo* using a gamma probe. In this context, different imaging modalities, more specifically CEUS, have been investigated in swine melanoma models and in clinics (Ungureanu, et al. 2016).

Goldberg *et al.,* investigated the performance of CEUS (also termed lymphatic ultrasonography or lymphosonography) for the detection of lymphatic channels, SLNs, and metastases after the peritumoral administration of MBs in a swine melanoma model (Goldberg, et al. 2011, Goldberg, et al. 2004). They reported that CEUS detected half as many false positives as lymphoscintigraphy did. The accuracy of SLN detection was 81.8% and 63.2% for CEUS and lymphoscintigraphy, respectively. The accuracy of CEUS for SLN characterization was 80%. However, when the size of the enhanced SLNs was considered in the characterization

of SLNs, the accuracy was 86%. These results suggest that CEUS is statistically more efficient than lymphoscintigraphy in SLN detection in preclinical models. Nevertheless, the efficiency of CEUS for SLN characterization (benign versus malignant) is limited. Recently, Bertelsen *et al.,* confirmed these results and suggested that CEUS may be useful for accurate SLN dissection (**Figure 4**) (Bertelsen, et al. 2019). Moreover, Liu *et al.,* reported that secondary LNs can also be detected with CEUS after direct injection of MBs into contrast-enhanced SLNs (Liu, et al. 2014). Secondary LNs detected using CEUS were nearly five times more likely to contain melanoma metastases than those removed using radical LN dissection. Recently, Nam *et al.,* investigated the performance of molecular US imaging with dual-targeted MBs to detect melanoma metastases in SLNs in a swine melanoma model (Nam, et al. 2018, Nam, et al. 2019). These MBs were functionalized with $\alpha v\beta_3$ integrin and P-selectin antibodies and injected intravenously. They reported that molecular US imaging had higher sensitivity (91% versus 80%) and specificity (67% versus 54%) than B-mode imaging for the diagnosis of metastatic LNs (Nam, et al. 2019). The mean contrast intensity from the dual-targeted MBs for metastatic SLNs was 6-fold higher than that of benign LNs, whereas control MBs (*i.e.,* IgG-labeled MBs) showed no significant difference in contrast intensity between metastatic and benign LNs (Nam, et al. 2018).

Despite the high sensitivity of CEUS for SLN detection in swine melanoma models, the first clinical study showed contradictory results. Indeed, Schmid-Wendtner *et al.,* demonstrated that i.v. injection of UCAs for color Doppler imaging in 19 patients with cutaneous melanoma provided additional information on the morphological aspects of vascularity for the discrimination of malignant LNs from reactive LNs, hematomas, or seromas (Schmid-Wendtner, et al. 2002). CEUS revealed perfusion primarily in peripheral areas of LN metastases or in a mixed pattern with high perfusion in one region and lack of perfusion in another. However, Nielsen *et al.,* reported that SLNs were visualized only in 1 patient out of 10 with

melanoma, thus suggesting that CEUS might not be used for SLN detection in clinics (Nielsen, et al. 2009). They explained the following: i) sows and humans have different LN structures and afferent lymphatic vessels, and ii) the echogenicity of the hilum is more hyperechoic in humans than in sows. Consequently, it is difficult to determine whether this hyperechogenicity is physiologically normal or induced by UCAs; iii) Sonazoid® (Goldberg, et al. 2011, Goldberg, et al. 2004) and Levovist® (Schmid-Wendtner, et al. 2002) fill the LNs more efficiently than SonoVue® thus providing higher contrast to the surrounding tissues (Nielsen, et al. 2009). In this analysis, the administration ways of UCAs are not discussed. Indeed, UCAs were injected peritumorally in swine melanoma models (Goldberg, et al. 2011, Goldberg, et al. 2004) while they are administered either subcutaneously (Nielsen, et al. 2009) or intravenously (Schmid-Wendtner, et al. 2002) in clinical trials. The contradictory results observed between preclinical and clinical studies could be also explained by the different administration ways of UCAs used in both type of studies. Other clinical investigations have been conducted to assess the performance of CEUS for SLN detection in melanoma patients after an i.v. injection of UCAs. De Giorgi *et al.,* found that CEUS showed a negative predictive value of 100% in a sample of 15 patients with melanoma (De Giorgi, et al. 2010). These data indicate that all negative results were confirmed by negative SLN histopathological analysis; thus, the SLNs were nonmetastatic. Nevertheless, CEUS has a high false positive rate for SLN detection. This modality identified eight out of 13 histologically confirmed negative SLNs, with a specificity of 61.5%. On CEUS, these five false-positive SLNs were categorized as suspicious (4/5) or positive (1/5). This investigation is the first to report a sensitivity of 100% and an accuracy of 73.7% for CEUS in diagnosing metastases in the SLNs of melanoma patients (De Giorgi, et al. 2010). In addition, Rubaltelli *et al.,* performed CEUS examinations in a series of 436 melanoma patients after standard US imaging to assess the significance of focal thickening of the superficial LNs in patients with cutaneous melanoma (Rubaltelli, et al. 2011). The CEUS

findings were compared with the results of fine-needle aspiration cytology (FNAC). CEUS correctly categorized 42 of 44 LNs showing focal cortical thickening with a sensitivity of 100%; more importantly, the specificity was 99.5 %. This sensitivity was higher than that of standard US imaging (93%). In 29 nodes, the area of focal thickening displayed a contrast enhancement comparable to that of the remaining cortex. In 15 nodes, this area was less perfused than the adjacent parenchyma during the arterial phase. Some areas showed perfusion defects during the parenchymal phase. Their results showed 13 true positives, 31 false positives, and no false negatives. FNAC should only be performed in 15 of 44 patients and avoided in 29 patients with negative results on both CEUS and histopathological examinations. Two years later, Rubaltelli *et al.,* investigated the performance of CEUS in the differential diagnosis of benign and malignant LNs based on the enhancement in the blood stream pattern on CEUS (Rubaltelli, et al. 2014). In 47 of 540 patients, US examination of LNs revealed an absence of echogenic hilus, round shape, and peripheral capsular vascularity. CEUS revealed altered blood perfusion in the LNs. US-FNAC confirmed the presence of LN metastasis in these patients. In 442 of 540 patients, the size, morphology, and vascularity of the LNs were characteristic of benign LNs. In 51 of 540 patients, standard US imaging showed LNs with focal cortical lobulation. On CEUS imaging, no perfusion defect was observed in 26 of the 51 patients, and US-FNAC revealed the absence of metastases in the LNs. In 25 of the 51 patients, CEUS showed defects in the blood perfusion of the LNs. Using US-FNAC, the presence of metastases in the LNs was confirmed in 19 of 25 patients and was excluded in 6 of 25 patients. Considering the morphological parameters (*i.e.,* echogenic hilus, round shape, and peripheral capsular vascularity), standard US imaging had a sensitivity, specificity, and accuracy of 71%, 100%, and 97%, respectively. This imaging modality showed 19 false negatives and no false positives. If the presence of focal cortical thickening was considered as a malignancy criterion, the sensitivity, specificity, and accuracy were then 100%, 93%, and 94%, respectively. This

modality yielded 32 false positives and no false negatives. However, when CEUS was combined with standard US imaging to examine LNs with focal cortical thickening, the sensitivity and the specificity were 98% and 99%; more importantly, the accuracy was 99%. The combination of both imaging modalities accurately categorized 534 of 540 melanoma patients, but revealed six false positives and no false negatives. The likelihood ratios established the good performance of the imaging modalities exploited in this clinical trial and the superiority of CEUS in comparison with the recommended values of above 10 and below 0.1 for positive and negative likelihood ratios, respectively.

Altogether, these preclinical and clinical data suggest that CEUS (with bare or targeted MBs) is a promising imaging modality for specifically detecting metastatic SLNs and secondary LNs and quantifying the degree of metastatic involvement.

Liver

The liver is the main solid organ in the abdomen where melanoma metastases have been discovered. Contrast-enhanced CT is the most common imaging modality used to examine liver metastases (Barat, et al. 2021). However, MRI has been described to be more sensitive than CT for the detection of liver metastases (Sofue, et al. 2012). Although US and PET imaging may also help to examine liver metastases, both modalities are reported to be less sensitive than CT and MRI because of operator dependence and the low spatial resolution of US (Chang, et al. 2014) and PET imaging (Barat, et al. 2021), respectively. Liver metastases are mostly well-defined and hypoechoic lesions observed on US imaging. However, diffuse hepatic infiltrations of melanoma metastases, as well as very large metastatic lesions, can induce a heterogeneous echotexture with diffusely increased echogenicity, suggesting hepatocellular carcinoma or cirrhosis (Velazquez, et al. 2019). As previously described (Lu, et al. 2019), CEUS is an effective modality for the detection and characterization of liver metastases, which are smaller in size and more frequent than B-mode imaging. CEUS displayed a transient and homogenous

arterial contrast enhancement in melanoma liver metastases, followed by rapid and complete wash-out initiated within the conventional arterial phase (Murphy-Lavallee, et al. 2007). This enhancement pattern was similar to that obtained using MRI and CT imaging. In addition, malignant liver lesions are hypoechoic in the late contrast phase on CEUS compared to healthy liver tissue, whereas benign lesions appear isoechoic or hyperechoic (Quaia, et al. 2004, Wildner, et al. 2019). Corvino *et al.,* reported that CEUS is a promising imaging modality for diagnosing metastatic cystic liver lesions, especially melanoma (Corvino, et al. 2016). Such lesions are rare, and their differential diagnosis is not easy compared to other liver metastases. They described the case of a 41-year-old patient with a rectal melanoma with solitary complex cystic liver metastasis. CEUS revealed some distinctive features of healthy liver parenchyma. This diagnosis was confirmed using ultrasound-guided FNAC. CEUS made it possible to establish a correct and early diagnosis and to provide appropriate management for the patient.

Gallbladder

With 50%–65% of all metastatic lesions involving the gallbladder, melanoma is the most common cause of gallbladder metastases (Backman 1969). Because such metastases are rare and frequently asymptomatic or rarely associated with obstructive symptoms or acute cholecystitis, their clinical diagnosis can be challenging (Chang, et al. 2014). Clinicians or radiologists can confuse tumor nodules with gallbladder sludge or pay little attention to them (Barretta, et al. 2011). Although most patients with gallbladder metastases have widespread cancer and poor survival, the gallbladder may represent the first metastatic site in a few patients (Barretta, et al. 2011). These rare cases can be treated surgically if they are diagnosed correctly at an early stage (Katz, et al. 2007). As previously reported, US imaging is an effective modality for detecting and characterizing gallbladder metastases (Holloway and King 1997). These metastases appear as single or multiple moderate/hyperechoic lesions (> 1 cm in diameter) attached to the gallbladder wall. These nodules display minimal to absent posterior acoustic

shadowing. In addition, gallbladder wall thickening is diffuse in cases of tumor infiltration or associated cholecystitis. Gallbladder metastases are known to be perfused. Indeed, Barretta *et al.,* reported that CEUS showed early, intense, and diffuse contrast enhancement of metastatic lesions in eight patients with primary melanoma gallbladder metastases (Barretta, et al. 2011). This enhancement gradually decreased over several minutes after i.v. injection of UCAs. Andreano *et al.,* described a rapid, intense, but heterogeneous contrast enhancement during the arterial phase and a very rapid wash-out at 60 s after i.v. contrast administration to be indicative of a malignant lesion (**Figure 5**) (Andreano, et al. 2010). In addition, Barretta et *al.,* demonstrated that color Doppler imaging failed to detect any blood perfusion in the gallbladder metastases of 5/11 patients with primary melanoma gallbladder metastases (Barretta, et al. 2011). In three of these patients, CEUS showed a significant contrast enhancement of the metastatic lesions, suggesting that these lesions were indeed perfused. The detection of flow signals in color Doppler after i.v. contrast injection in two of these three patients confirmed that CEUS is more sensitive than color Doppler. Overall, these clinical results demonstrate that CEUS is a complementary US imaging modality for precisely identifying metastatic gallbladder metastases.

CEUS-guided interventions

As previously described, US-guided biopsy (*e.g.,* core needle biopsy and SLNB) is an accurate and safe method for obtaining tissue samples for the histopathological diagnosis of melanoma (**Table 2**). When using CEUS, the tumor should be biopsied in the most significant areas (*e.g.,* areas of angiogenesis) to provide an accurate histological diagnosis of the tumor. CEUS-guided core needle biopsy has provided promising results in the diagnosis of soft tissue tumors (Coran, et al. 2015). Indeed, De Marchi *et al.,* reported that 94.8% of tumor samples were adequate for diagnosis with 97.1% sensitivity and 92.5% specificity (De Marchi, et al. 2010). To the best of our knowledge, no study has been conducted on the diagnosis of melanoma. Consequently,

further clinical studies are needed to assess the performance of CEUS-guided biopsy in the detection and characterization of melanoma.

Conventional intraoperative US imaging is an inexpensive and safe method that allows visualization of real-time changes in tumor lesions during surgical intervention. Unlike CEUS, this modality does not provide functional or perfusion information, which may be useful for discriminating normal tissues from tumor tissues. Therefore, CEUS is a promising tool for use in intraoperative imaging. Lekht *et al.,* reported the use of real-time intraoperative CEUS in cranial neurosurgery for metastatic melanoma (Lekht, et al. 2016). This lesion showed a real-time dynamic tumor perfusion pattern that was inconsistent with the previously described patterns of brain tumors. After resection of the lesion, CEUS detected a residual tumor in an unsafe brain location for additional resection. In this clinical study, intraoperative CEUS assisted maximal tumor resection with no intraoperative complications. In agreement with previous studies (Prada, et al. 2014), this study confirmed that intraoperative CEUS is a safe, real-time, and dynamic contrast-based imaging technique to guide surgery and biopsy in neuro-oncology. Further prospective investigations should determine the place of this modality in the diagnostic arsenal and therapeutic management of melanoma.

CEUS monitoring of therapeutic follow-up

Since the development of new targeted therapies (*i.e.,* therapeutic antibody, tyrosine kinase inhibitors, *etc.*) and US therapies (*i.e.,* high-intensity focused ultrasound, antivascular ultrasound therapy, *etc.*), it has been clearly established that the assessment of morphological tumor criteria (*e.g.,* tumor dimensions and volume) alone cannot determine the early therapeutic efficacy of these treatments (Lassau, et al. 2010). Indeed, morphological evaluation of tumors does not reveal early physiological changes in tumors. Some preclinical and clinical studies have reported that melanoma is susceptible to treatment with antiangiogenic drugs (*e.g.,* sorafenib, bevacizumab, and imatinib) (Flaherty, et al. 2015, Forsberg, et al. 2014, Leguerney,

et al. 2012, Seiler, et al. 2007) or with therapeutic US (Rouffiac, et al. 2006, Wood, et al. 2009), which leads to a decrease in tumor angiogenesis, followed by tumor hypoxia and cell death. As previously reported (Ferrara, et al. 2000), Doppler imaging is not very sensitive and accurate for assessing the effects of these treatments on slow blood flow in tumor vessels. However, CEUS allows the visualization and quantification of tissue vascularity with high sensitivity (Escudier, et al. 2007, Lavisse, et al. 2008).

The contribution of CEUS imaging to targeted treatment assessment has been extensively described and discussed by Lassau *et al.,* highlighting CEUS as a powerful and relevant functional modality for monitoring targeted treatments (**Table 2**) (Escudier, et al. 2007, Lavisse, et al. 2008, Leguerney, et al. 2012). Indeed, CEUS enables the detection of tumor microvessels and the quantitative evaluation of tumor perfusion using raw linear data. This modality allows the calculation of perfusion parameters, including blood flow and blood volume, which correspond to the slope of wash-in and the area under the time–intensity curve (AUC) on the time–intensity curve, respectively. Thus, Lavisse *et al.,* investigated the early tumor vasculature disrupting effects of a pharmacological agent, AVE8062, using CEUS imaging in a murine B16F10 melanoma model (Lavisse, et al. 2008). They reported that DCEUS allowed for an effective and quantitative assessment of the anti-angiogenic effects of AVE8062. Variations in tumor perfusion parameters were positively correlated with changes in microvascular density. Similarly, Forsberg *et al.,* described that CEUS is a sensitive modality for investigating the functional effects of VEGF traps on tumor neovascularity in a DB-1 human melanoma xenograft model (Forsberg, et al. 2014). A strong correlation between DCEUS and the histological measures of angiogenesis has also been reported. These preclinical data are supported by clinical trials. Lassau *et al.,* demonstrated that a decrease in tumor angiogenesis can be discerned and measured in responders after one or two treatment weeks (Lassau, et al. 2007, Lassau, et al. 2010). This decrease is generally correlated with progression-free and

overall survival in renal cell and hepatocellular carcinomas. Flaherty *et al.,* hypothesized that significant changes in tumor vasculature assessed by CEUS (and DCE-MRI) would correlate with the clinical efficacy of imatinib and bevacizumab in patients with advanced melanoma and other advanced cancers (Flaherty, et al. 2015). However, only a few patients showed evidence of disease control. Indeed, of the five patients imaged with CEUS before and after the therapeutic regimen, two patients showed a significant decrease in tumor perfusion, one patient showed a minor decrease in tumor perfusion, and two patients exhibited no change in tumor perfusion. Consequently, no correlation between the clinical efficacy of the treatment and changes in tumor vasculature could be established. Nevertheless, Lassau *et al.,* reported a multicenter investigation of the performance of CEUS to assess tumor response in different solid tumor types, including melanoma, treated with several anti-angiogenic drugs (*e.g.,* sorafenib, bevacizumab, sunitinib, and imatinib) (Lassau, et al. 2014). In this clinical study, they performed 1968 CEUS examinations in 539 patients, including 55 patients with melanoma. They demonstrated that CEUS provides a predictive biomarker of tumor progression related to blood volume, termed as the change in AUC from baseline to day 30. Indeed, patients with a greater than 40% decrease in AUC on day 30 showed better freedom from progression and overall survival. These data suggest that this biomarker should be considered for the early evaluation of anti-angiogenic treatment of melanoma.

In conclusion, preclinical studies have clearly demonstrated that CEUS is a relevant diagnostic tool for assessing the early effects of antiangiogenic treatments in melanoma. However, further investigations are required to demonstrate its clinical relevance.

DRUG DELIVERY USING MICROBUBBLE-ASSISTED ULTRASOUND

Thus, MB-assisted US (*i.e.,* sonoporation or sonopermeabilization) is a noninvasive and local drug delivery method that offers great promise for improving the therapeutic efficacy of a wide range of therapeutic molecules (*e.g.,* chemotherapeutics, antibodies, recombinant

peptides/proteins, and nucleic acids) by enhancing their bioavailability in tumor tissues and reducing their systemic side effects on healthy tissues (Kooiman, et al. 2020). For their *in-vivo* delivery, these molecules are either co-administered with MBs or loaded on or into MBs (Kooiman, et al. 2020). After in *in-vivo* administration and sufficient accumulation of therapeutic molecules and MBs in the tumor microvasculature, the tumor tissue is exposed to US waves (Presset, et al. 2020). Under the action of US, volumetric oscillations of MBs induce several local acoustic phenomena close to the endothelial wall of tumor vessels, which results in their transient permeabilization (Presset, et al. 2020). This vascular permeabilization significantly enhances extravasation, penetration, and retention of therapeutic molecules in tumor tissues (Kooiman, et al. 2020, Presset, et al. 2020). Thus, MB-assisted US is an easy-to-use and cost-effective delivery method for therapeutic molecules, including chemotherapeutic drugs (Baghirov, et al. 2018, Prasad and Banerjee 2019, Prasad, et al. 2020), photothermal agents (Hu, et al. 2020, Liu, et al. 2019, Wang, et al. 2014), melanoma-associated antigens (Ags), and immunomodulatory molecules (Dewitte, et al. 2014, Gao, et al. 2018, Oda, et al. 2012) into melanoma. In addition, this method may be used to treat primary cutaneous melanoma as well as metastases located in deep tissues under the guidance of US imaging (Sennoga, et al. 2017).

In this section, we provide only a survey of preclinical studies exploring the therapeutic efficacy and safety of delivery of therapeutic molecules using MB-assisted US for the treatment of melanoma because no clinical investigation has been conducted to the best of our knowledge.

Chemotherapy

Conventional anti-cancer chemotherapy is ineffective in treating advanced melanoma. Since 2006, some investigations have been performed to design therapeutic protocols for acoustically mediated delivery of free or encapsulated forms of chemotherapeutics in mouse models of primary tumors and metastases of melanoma (Abdalkader, et al. 2015, Prasad and Banerjee

2019, Tartis, et al. 2006) (**Table 3**). Among these anti-cancer drugs, doxorubicin (DOX) is one of the most potent and is administered alone or in combination with other drugs for the treatment of solid tumors (Carvalho, et al. 2009). However, its clinical use is severely limited owing to its systemic side effects and, specifically, its cardiotoxicity. To overcome this issue, DOX was encapsulated inside PEGylated liposomes (Doxil® or Caelyx®) (Barenholz 2012). These DOX liposomal formulations passively accumulate inside the tumor through enhanced permeability and retention effects (Barenholz 2012), thus significantly reducing the cardiotoxicity of DOX. However, several investigations have reported other adverse effects (*e.g.,* mucositis and hand–and-foot syndrome) and a limited intratumoral (i.t.) DOX concentration (O'Brien, et al. 2004). One of the strategies to overcome both problems consists of loading DOX inside or onto MBs and then intravenously administering these DOX-loaded MBs before exposing the tumor tissues to US. Accordingly, Abdalkader *et al.,* designed a novel phospholipid-based MB formulation containing DOX for an acoustically mediated drug delivery (2 MHz, 2 W/cm^2, 50% DC, 10 Hz PRF) in B16BL6 melanoma mouse model (Abdalkader, et al. 2015). Nine days after tumor inoculation, the tumors were treated three times over 2 d intervals. Mice received an i.v. injection of DOX-loaded MBs (70 μg DOX/330 μg lipid in 200 μL of 5% glucose solution), and the tumors were immediately exposed to US for 60 s. The results showed that acoustically mediated delivery using DOX-loaded MBs, as compared to DOX-loaded MB treatment alone (*i.e.,* without US exposure; 0.100 μg/g tumor tissue), significantly enhanced the i.t. DOX dose (0.536 μg/g tumor tissue) (**Figure 6A**). Because cardiotoxicity is a major side effect of DOX, the authors assessed the DOX dose in the heart tissue. Surprisingly, there was no significant change in DOX doses in the heart and liver tissues between the experimental groups (**Figure 6B-C**). Unfortunately, they did not assess the levels of creatine kinase, alanine, and aspartate aminotransferases to evaluate the effects of this treatment on heart and liver functions. In addition, acoustically mediated DOX delivery using

DOX-loaded MBs significantly induced a reduction in tumor volume (2453.9 ± 175 mm^3) by day 27 after tumor inoculation compared with no treatment (7156.2 ± 1384 mm^3) and DOX-loaded MB treatment alone (*i.e.,* without US exposure; 4663.2 ± 454 mm^3) (**Figure 6D**). Furthermore, treatment with DOX-loaded MBs in combination with US exposure did not induce any significant loss in body weight relative to no treatment or DOX-loaded MB treatment alone, suggesting that this treatment was well tolerated (**Figure 6E**). Altogether, these results demonstrate that the combination of DOX-loaded MBs with US is an efficient and safe strategy for delivering DOX to primary melanoma tumors.

Moreover, Prasad *et al.,* developed different formulations to deliver or co-deliver curcumin (Cur) using MB-assisted US into melanoma (Prasad and Banerjee 2019, Prasad, et al. 2020). Cur is a plant-derived anticancer agent with negligible side effects. Preclinical studies have reported that the high therapeutic efficacy of Cur requires higher doses because of its low solubility and bioavailability (Heger, et al. 2014). To overcome these issues, Cur has been encapsulated inside polymer-or phospholipid-based colloidal particles. Prasad *et al.,* designed a Cur-encapsulated lecithin nanoemulsions (Cur-NE) for the oral administration of Cur (Prasad, et al. 2020). They then investigated MB-assisted US as a physical method to improve the spatiotemporal delivery of Cur into the tumor in a B16F10 melanoma mouse model. Cur-NE was administered orally at 40 mg/kg b.w. to mice with subcutaneous (s.c.) melanoma. Two hours later, MBs (250 μg) were intravenously injected. The tumors were immediately exposed to US (2 W/cm^2, 50% DC) for 60 s. Mice were treated five times: first three treatments on alternate days and the last two treatments after a duration of two days. Fifteen days after treatment initiation, this protocol significantly reduced the relative growth rate of the tumor 8-fold and 10-fold compared to Cur-NE treatment alone or free Cur treatment alone, respectively. The Kaplan–Meier survival study revealed the survival percentage was 90.9% in the mice group treated with Cur-NE and MB-assisted US, whereas this percentage was 75.6% in the mice group

receiving free Cur treatment alone. Unfortunately, the authors did not describe the survival percentage in mice treated with Cur-NE alone. Nevertheless, these results clearly established that MB-assisted US significantly improved the therapeutic efficacy of Cur in a mouse model of melanoma. In addition, Prasad *et al.,* developed a new MB formulation to codeliver both anticancer drugs, *i.e.,* Cur and topotecan (Tpt) (Prasad and Banerjee 2019). Topotecan is a hydrophilic analog of camptothecin, which prevents DNA replication by inhibiting topoisomerase I activity. They designed polymeric nanocapsules with a hydrophobic core and hydrophilic polymeric shell, thus enabling the loading of Cur and Tpt, respectively (Prasad and Banerjee 2019). These nanocapsules were then loaded onto the surface of the MBs (Tpt/Cur-loaded MBs). Such nanocapsule/MB complexes are more stable than liposome/MB complexes and are more suitable for the coencapsulation of hydrophobic and hydrophilic drugs. The authors investigated the therapeutic efficacy of the codelivery of Tpt and Cur using Tpt/Cur-loaded MBs in combination with US (2 W/cm^2, 50% DC) in the B16F10 melanoma tumor model. Fifteen days after tumor inoculation, Tpt/Cur-loaded MBs (5 mg/kg and 2.5 mg/kg for Cur and Tpt, respectively) were intravenously injected, and the tumors were immediately exposed to US for 60 s. Mice were treated five times as described above. The codelivery of Tpt and Cur using Tpt/Cur-loaded MBs in combination with US induced a 15-fold and 4-fold decrease in the relative growth of tumors compared to free Tpt/Cur treatment alone and Tpt/Cur-loaded MBs treatment alone, respectively. Further, the mice group receiving Tpt/Cur-loaded MBs treatment (without US exposure) or free Tpt/Cur treatment on its own showed a survival rate of 93.7% and 26.2%, respectively. Surprisingly, the authors did not report the effects of Tpt/Cur codelivery using Tpt/Cur-loaded MBs in combination with US on mouse survival. However, this preclinical study is the first to demonstrate the potential of MB-assisted US to co-deliver more than one anticancer drug for the treatment of melanoma.

In conclusion, preclinical studies have successfully reported the therapeutic benefits of MB-assisted US in the delivery of one or more chemotherapeutics in s.c. melanoma murine models. These findings should be confirmed in small- and large-animal models of primary tumors and metastases of melanoma. In addition, the contribution of host immunity to the tumor response to chemotherapy after acoustically mediated drug delivery is still lacking and needs to be investigated in complementary studies using syngeneic animal models of melanoma.

Photothermal therapy

Photothermal therapy relies on the use of a femtosecond pulse laser to cause irreversible thermal damage to tumor tissues (Li, et al. 2020). This therapeutic modality is a promising and noninvasive strategy for the treatment of isolated cutaneous melanoma (Liu, et al. 2019). However, conventional laser irradiation cannot treat deep tumor tissues and generally induces thermal damage to the healthy tissues surrounding the tumor lesion (Li, et al. 2020). To solve this problem, photothermal agents (*e.g.,* indocyanine green, IR780 dye, gold nanorods, melanin) are loaded in acoustically responsive carriers (*e.g.,* MBs, nanodroplets) to enhance the delivery of these agents into melanoma after US exposure (**Table 4**). The accumulation of such carriers can be significantly increased in the melanoma microvasculature by functionalizing these carriers with targeting agents (*e.g.,* cyclic arginine-glycine-asparagine, antiVEGFR2 antibody), which bind overexpressed endothelial biomarkers (*e.g.,* integrin $\alpha v\beta_3$, VEGFR2). This enhanced i.t. bioavailability of photothermal agents improves the thermal efficacy of the pulse laser, thus irreversibly ablating superficial melanoma (Hu, et al. 2020, Wang, et al. 2014).

Wang *et al.,* loaded photoabsorbing agents, namely gold nanorods, in VEGFR2-targeted MBs to effectively deliver these agents into melanoma cells using MB-assisted US, thus improving the efficacy of plasmonic photothermal therapy (Wang, et al. 2014). Once administered intravenously (200 μL at 6.8×10^8/mL containing 10 nM gold nanorods), these MBs bound VEGFR2 overexpressed in the melanoma microvasculature in mice (B16F10).

Exposure of the tumor to US (1 MHz, 100 Hz PRF, 20 cycles, 2.98 MPa for 5 min) induced MB destruction, which permeabilized its microvasculature and released gold nanorods into the tumor tissue. Despite showing that MB-assisted US significantly increased the i.t. bioavailability of gold nanorods, the authors did not demonstrate that this process is associated with an improvement in the effectiveness of photothermal therapy. Indeed, in a mouse breast adenocarcinoma model, the authors reported a significant laser-mediated temperature increment (> 45 °C) to eradicate the tumor after the acoustically enhanced i.t. delivery of gold nanorods (Wang, et al. 2014). Moreover, Hu *et al.,* designed melanin-cored (*i.e.,* photoabsorbing agent) and DOX-loaded (*i.e.,* chemotherapeutics) perfluoropentane nanodroplets for the photothermal therapy of melanoma in a mouse model (A375) (Hu, et al. 2020). After their i.v. or i.t. injection (200 μL containing 10 mg/mL melanin and 110 μg/mL DOX), the tumor tissue and, therefore, circulating nanodroplets were exposed to an optoacoustic synergistic irradiation (*i.e.,* laser at 1 $W.cm^{-2}$; US at 1.1 MHz, 1 Hz PRF, 5 cycle/pulse, 0.82 MPa PNP, for 2 min). This method vaporized these nanodroplets into MBs, which cavitated to increase the permeability of the tumor microvasculature, thus enhancing the i.t. delivery of melanin and DOX. These molecules mediated a secondary chemo-photothermal therapy under subsequent laser irradiation (1 $W.cm^{-2}$ for 5 min; 24 or 5 h after i.v. or i.t. injection of nanodroplets, respectively), which efficiently eradicated the melanoma. These investigations show that photothermal therapy in combination with or without chemotherapy could have great potential for the treatment of melanoma. Nevertheless, additional studies must be performed in small and large animals to confirm the therapeutic benefits of this therapy in melanoma treatment.

Immunotherapy and Vaccination

Immunotherapy and vaccination are promising therapeutic modalities for producing potent and long-lasting immunizations against melanoma (Escoffre, et al. 2016). Immunotherapy

stimulates the immune response in melanoma patients by administering immunomodulating molecules (*i.e.,* interferons, interleukins, antiPD1/PDL1, and antiCTLA4 antibodies) (Yamaguchi, et al. 2011). Moreover, prophylactic and therapeutic vaccines have been designed and evaluated for melanoma treatment. Prophylactic immunization relies on the delivery of melanoma-associated antigens (MAA) in healthy patients to induce a rapid and efficient immune response during disease occurrence (Un, et al. 2011). In addition, as an immunotherapy, the therapeutic vaccine aims to stimulate the immune response in diseased patients by delivering MAA (Gao, et al. 2018, Oda, et al. 2012). Immunomodulating molecules and MAA can be administered either as recombinant peptides/proteins or as encoded by plasmid DNA (pDNA) or messenger RNA (mRNA). Nevertheless, the pharmacological, immunological, and physicochemical properties of these molecules limit their access to target tissues (*e.g.,* immune cells, LN, skin, skeletal muscle, and melanoma), thus reducing their therapeutic efficacy (Escoffre, et al. 2016). As previously described for chemotherapy, the clinical development of anti-cancer immunotherapy and vaccination requires the design of a safe and efficient method for the delivery of these molecules. In the remainder of this section, we demonstrate the potential of MB-assisted US for the delivery of these molecules for the treatment of melanoma (**Table 5**).

Cytokine pDNA-based immunotherapy

Cytokine pDNA-based immunotherapy (*e.g.,* interferon-γ, interleukin-2, -12 and -27, *etc.*) is a promising strategy for inducing long-lasting antitumor immunity against primary and metastatic cancer diseases (Escoffre, et al. 2016). The delivery of cytokine pDNA can result in complete tumor regression, inhibition of metastasis, and increase in survival. This strategy is well tolerated in comparison to immunotherapy based on the use of recombinant cytokines. Indeed, Yamaguchi *et al.,* reported the therapeutic effects of the delivery of interferon-γ pDNA using MB-assisted US (1 MHz, 0.5 Hz PRF, 50% DC, 0.22 $W.cm^{-2}$, for 3 min; i.t. injection of

100 μg pDNA/100 μL Sonazoid MBs) in a melanoma mouse model (C32) (Yamaguchi, et al. 2011). Two weeks after tumor inoculation, the tumors were treated once a week for four weeks. This strategy led to a 2-fold decrease in tumor growth compared to unsonicated tumors. Histopathological examination of tumor tissues (*i.e.,* terminal deoxynucleotidyl transferase (TDT)-mediated dUT nick end labeling assay and immunohistochemistry against interferon-γ and caspase-3) confirmed the therapeutic efficacy of this immunotherapy. Although these results may demonstrate that cytokine pDNA-based immunotherapy has great potential for the treatment of melanoma, regrettably, the delivery of cytokine pDNA using MB-assisted US has been poorly investigated for the treatment of melanoma, whereas it has been described for the treatment of other types of cancers (Suzuki, et al. 2010, Zolochevska, et al. 2011).

Recombinant vaccines

The development of antitumor vaccines has become a major research topic in the field of cancer immunotherapy. Tumor-specific antigens are the main components of tumor vaccines. They induce specific Th-1 and Th-2 immune responses to inhibit tumor occurrence and development. Melanoma-associated antigen A1 (MAGEA1), gp100, melanoma antigen recognized by Th-1 cells (MART-1), and tyrosinase-related protein (TRP) are the main MAA exploited in recombinant vaccines (Gao, et al. 2018, Un, et al. 2011). MAGEA1 is processed and presented by major histocompatibility complex-1 (MHC-1) molecules on cancer cells and induces a Th-1 immune response against MAGEA1-expressing cancer cells. However, MAGEA1-based tumor vaccines do not show significant clinical effects on cancer (Slingluff, et al. 2008). To overcome this issue, MAGEA1 is fused with heat shock protein 70 (HSP70) to improve the processing and presentation of MAGEA1, thereby significantly enhancing Th-1 and Th-2 immune responses against melanoma. Gao *et al.,* proposed the delivery of this HSP70/MAGEA1 fusion protein using MB-assisted US (MI 0.75; s.c. injection of 10 μg/100 μL/mouse of HSP70/MAGEA1-loaded MBs) in a mouse melanoma model (B16-MAGEA1)

(Gao, et al. 2018). To achieve this goal, HSP70/MAGEA1-loaded MBs were developed. One week post-tumor inoculation, MBs were subcutaneously administered around the LNs under US imaging guidance. The HSP70/MAGEA1 fusion proteins were then released from the MBs after US exposure. This immunization protocol was repeated once a week for three weeks. This strategy enhanced Th-1 and Th-2 immune responses more effectively than the HSP70/MAGEA1 fusion protein alone. Used as a therapeutic recombinant vaccine, this immunotherapy induced 8-fold and 2-fold decreases in tumor volume compared to mice treated with MBs or HSP70/MAGEA1 fusion protein alone, respectively. This result translated into a significant increase in survival for mice immunized with this vaccine (50% survival at 60 d post-tumor inoculation) in comparison with mice treated with HSP70/MAGEA1 fusion protein (10% survival at 52 d post-tumor inoculation) and MBs only (no living mice 28 d post-tumor inoculation). In addition, this strategy provides an efficient prophylactic vaccine against melanoma. Indeed, this vaccine resulted in a 4-fold and 2-fold decrease in tumor volume compared to mice treated with MBs or HSP70/MAGEA1 fusion protein alone, respectively. Subsequently, immunized mice showed prolonged survival (35% survival at 70 d post-tumor inoculation) in comparison with those immunized with the HSP70-MAGEA1 fusion protein (20% survival at 58 d post-tumor inoculation) or MBs only (no living mice 25 d post-tumor inoculation). These results demonstrate that MB-assisted US is a promising method for delivering recombinant vaccines, thus increasing their prophylactic and therapeutic efficacy.

Dendritic cell-based vaccines

Dendritic cells (DCs) are the most potent antigen-presenting cells (APCs) that prime and activate cytotoxic T-lymphocytes (CTL) and T-helper lymphocytes (*i.e.,* Th cells) (Abbas and Lichtman 2006). CTLs play a major role in the elimination of tumor cells, whereas Th cells support long-lasting and potent T and B lymphocyte responses. DCs also play a major role in the production of antibodies through their interactions with B lymphocytes. As sentinel cells of

our organism, DCs recognize, engulf, and process tumor antigens. DCs then migrate to draining LNs and mature into APCs. Mature DCs present epitope peptides derived from tumor antigens via MHC-I and MHC-II molecules, thus initiating the immune response. In addition, tumor antigens may directly access draining LNs, where resident DCs recognize them. Associated with danger signals, these agents trigger a suitable and effective adaptive immune response.

Based on these immunological properties, DC-based vaccines have been developed for melanoma treatment (Abbas and Lichtman 2006). Briefly, the DC precursors were purified from the patient after leukapheresis. Incubation of these precursors with different growth factors and cytokines (*e.g.,* granulocyte-macrophage colony-stimulating factor, and interleukin 4) generates immature DCs. Subsequently, DC maturation occurs when these cells are incubated with immunostimulatory cytokines (*e.g.,* Tumor necrosis factor α, interleukin 6, and FMS-like Tyrosine kinase 3 Ligand) and toll-like agonists (*e.g.,* lipopolysaccharides, CpG, and polyI:C). Mature DCs were loaded with MAA to generate activated DCs. These fully mature and activated DCs were administered back to the patient. Among the different methods for generating melanoma-specific DCs, bubble-assisted US can be used to deliver MAA and immunomodulating molecules as recombinant proteins/peptides or as encoded by pDNA or mRNA into DCs (Escoffre, et al. 2016). Oda *et al.,* designed a promising method to deliver directly MAA (50 μg) into DCs using US (2 MHz, 10% DC, burst rate 2 Hz, 2 $W.cm^{-2}$ for 3 × 10 s, with time interval of 10 s) and bubble liposomes (120 μg). This method directly delivered the MAA into the cytosol of DCs with an efficiency of approximately 74%, resulting in the presentation of MHC-I restricted Ags on DCs. To assess the efficacy of *in-vivo* prophylactic vaccination, mice were immunized twice with mature and activated DCs (1×10^6 cells/100 μL) at a one-week interval. B16/BL6 melanoma cells were then injected intravenously to generate lung metastases. DC-based vaccination induced a 4-fold decrease in the frequency of melanoma lung metastases (**Figure 7**). On the other hand, Dewitte *et al.,* preferred to deliver

both Ag (ovalbumin, used as Ag model) and immunomodulating mRNAs (TriMix: caTRL4, CD40-L, CD70) into DCs using MB-assisted US (1 MHz, 2 $W.cm^{-2}$, 20% DC, for 30 s; defined volume of MBs containing 10 μg ovalbumin (OVA) mRNA/40 μg TriMix) (Dewitte, et al. 2014). They then evaluated the efficacy of this DC-based vaccination in a mouse melanoma model (MO4) that overexpresses OVA. Ten days after s.c. inoculation of melanoma cells, mice were immunized twice by subcutaneously injecting mature and activated DCs (50 μL at 2×10^6 $cells.mL^{-1}$) at a one-week interval. These DCs induced a potent Ag-specific T cell response, leading to the specific lysis of melanoma cells. As a result, this DC-based vaccination resulted in a significant decrease in tumor growth, which naturally translated into an 82% prolongation of median survival for immunized mice in comparison with naive mice. Importantly, tumor eradication was observed in one-third of immunized mice that showed potent and long-lasting antigen-specific immunological memory. These preclinical studies show that bubble-assisted US is a promising method for delivering MAA and immunomodulating molecules into DCs.

DC-based vaccines are mainly generated *ex-vivo* from autologous DCs, which must be tailor-made for each patient. This process is complex and expensive, which prevents the generalization of immunotherapy. The *in-vivo* delivery of MAA and immunomodulatory molecules in APCs, including CDs and macrophages, bypasses these procedures (Un, et al. 2010). Accordingly, Un *et al.,* developed US-responsive and mannose receptor-targeted bubble lipoplexes that were selective to APC and carried pDNA encoding ubiquitylated MAA (*i.e.,* glycoprotein $gp100_{25\text{-}33}$ and tyrosinase-related protein $2_{181\text{-}188}$ peptide epitopes) (Un, et al. 2011). They investigated the efficacy of this strategy to induce a prophylactic immunization (1.045 MHz, 50% DC, 10 Hz burst rate, 1 $W.cm^{-2}$, for 2 min; i.v. injection of 400 μL bubble lipoplexes/50 μg pDNA) against primary and metastatic melanoma in a mouse model (B16BL6). To achieve this objective, the mice were immunized three times with a two-week interval between each immunization. Afterward, the mice were inoculated with melanoma cells

either subcutaneously to induce a subcutaneous tumor or intravenously to induce lung metastasis. The secretion of Th1 cytokines and CTL activities were significantly enhanced 10- and 15-fold in immunized mice compared to untreated mice at two weeks after the last immunization, respectively. In addition, the authors succeeded in obtaining potent and long-lasting (100 d post-tumor inoculation) immunization against primary cutaneous melanoma and melanoma lung metastases. Following investigation of this immunization against primary cutaneous melanoma, a complete tumor rejection was observed in 70% of immunized mice. These mice showed 80% survival rate at 100 d post-tumor inoculation, whereas no nonimmunized mice survived longer than 45 days post-tumor transplantation. In addition, this immunization significantly suppressed the formation of melanoma lung metastases in mice and induced a survival prolongation of immunized mice (75% survival at 100 d post-tumor inoculation) in comparison with naïve mice (no survival after 35 days post-tumor inoculation).

If this method induces an effective prophylactic immunization, its therapeutic efficacy for established melanomas is insufficient because the tumor growth rate is too fast for therapeutic immunization to be successful. The same research group proposed enhancing the *in-vivo* transfection efficacy of APCs to increase the efficacy of this therapeutic immunization. They reported that transfection efficacy was significantly increased by transcriptional activation using DOX -loaded liposomes (Un, et al. 2012). Indeed, DOX is known to activate transcription factors, such as nuclear factor kappa-light-chain-enhancer of activated B cells (NF-κB), thus increasing the transcription of transfected pDNA. Accordingly, they designed an immunization method associating the delivery of DOX-loaded liposomes (200 μL at 4 mg/kg b.w.) with APC transfection using mannose-targeted bubble lipoplexes (i.v. injection of 400 μL bubble lipoplexes/50 μg pDNA encoding $gp100_{25\text{-}33}$ and tyrosinase-related protein $2_{181\text{-}188}$ peptide epitopes) in combination with US (1.045 MHz, 50% DC, 10 Hz burst rate, 1 $W.cm^{-2}$, for 1 min) (Un, et al. 2011). DOX-loaded liposomes activated transcriptional factors (*e.g.,* NF-B and

activated Protein-1) in the spleen, and subsequently, pDNA expression was significantly enhanced in splenic cells. Moreover, this method resulted in an effective CTL response against tumor cells. To investigate the efficacy of this method in primary cutaneous melanoma, DOX-loaded liposomes were administered once a week after the s.c. inoculation of melanoma cells (B16BL6) in mice. Therapeutic immunization was performed twice, at 24 h and 2 weeks after the delivery of DOX-loaded liposomes. Only one immunization induced a 7-fold decrease in tumor volume compared to that in the nontreatment group. In addition, the survival of mice immunized twice was significantly prolonged (25% survival at 100 d post-tumor inoculation) in comparison with that of naïve mice (no survival after 40 d post-tumor inoculation). Using the previously described immunization schedule, mice immunized twice showed a lower number of lung metastases than the naïve mice. Taken together, these results demonstrate that the therapeutic effects of this immunization on established melanoma are significantly enhanced by the delivery of DOX-loaded liposomes.

In conclusion, bubble-assisted US is an effective method for the *ex-vivo* and *in-vivo* design of DC-based vaccines against melanoma. Current preclinical studies, mainly conducted in mouse melanoma models, should be confirmed in larger animals in the near future before clinical investigation.

FUTURE PERSPECTIVES AND CONCLUSIONS

Using bare or targeted UCAs enables CEUS to be utilized as a noninvasive and complementary imaging modality to US imaging for the detection and the characterization of primary cutaneous melanoma as well as metastatic melanoma (*e.g.,* LNs, liver and gallbladder). Indeed, high-resolution US imaging provides precise morphological (*e.g.,* dimensions and volume) and acoustic (*e.g.,* surface sound reflectance, intralesional sound reflection, and total US attenuation) characteristics, whereas CEUS provides more accurate and sensitive information on melanoma microvasculature than color/power Doppler imaging. Unfortunately, the studies

investigating the performance of CEUS for the detection and characterization of primary melanoma are mainly conducted on small- (mouse, rat) and large- (swine) animal models. Further clinical investigations should be performed to corroborate these preclinical studies and determine the performance of CEUS in a clinical context. Moreover, preclinical and clinical studies have revealed that CEUS is a promising imaging modality to specifically detect metastatic SLNs and secondary LNs and to measure the degree of metastatic involvement. Despite the low number of clinical studies, CEUS has also revealed several distinctive features in terms of tumor microvasculature between healthy liver and gallbladder tissues and metastatic foci present in these tissues. Because CEUS enables the early diagnosis of these metastases and provides the most adequate care for the patient, these results should be confirmed in large cohort clinical trials.

Anecdotally, few clinical studies have reported that CEUS can guide clinical interventions, including biopsy and surgery. Thus, CEUS-guided biopsy can provide an accurate histological diagnosis of melanoma by biopsying relevant tumor areas, such as those of tumor neoangiogenesis. In addition to conventional intraoperative US imaging, CEUS could provide perfusion information for helping surgeons to better discriminate healthy tissues from melanoma. Further investigations are needed to define the performance of CEUS in the supervision of diagnostic and therapeutic interventions. Furthermore, we have preclinically established evidence that CEUS is a sensitive and accurate US modality for assessing the early vascular changes induced by anti-angiogenic treatments of melanoma. These results have been partially confirmed in the clinical setting.

MB-assisted US is also an easy-to-use and cost-effective method for the noninvasive and local delivery of chemotherapeutic drugs, photothermal agents, melanoma-associated agents, and immunomodulating molecules into melanoma, which is achieved by increasing their extravasation and i.t. bioavailability and reducing their systemic side effects on healthy tissues.

This method provides the possibility of treating primary cutaneous and metastatic melanoma under the guidance of US imaging. However, we must keep in mind that current efficacy studies of acoustically mediated delivery have been reported in small animal models of primary and metastatic melanoma. Indeed, no proof of concept has been validated in preclinical studies on large animal models of melanoma or in clinical studies. Moreover, despite promising results, we can candidly question whether the acoustically mediated delivery of chemotherapeutic drugs and photothermal agents is relevant for the treatment of primary cutaneous melanoma. Indeed, recent skin removal of primary melanoma is minimally invasive, efficient, and safe. However, the activation and/or stimulation of the anti-tumor immune response by *in-vivo* acoustically mediated delivery of MAAs and immunomodulatory molecules showed promising results for the treatment of metastatic melanomas. The current data should be confirmed in small- and large-animal models of metastatic melanoma in the near future before clinical investigation.

FUNDING/SUPPORT

The IRIS project (2019-00131873) was supported by the Région Centre-Val de Loire (France) and was approved by the S2E2 cluster.

Conflict of Interest disclosure – The authors have no conflicts of interest to disclose.

REFERENCES

Abbas AK, Lichtman AH. Basic immunology: functions and disorders of the immune system. Philadelphia, USA: Saunders Edition, 2006.

Abdalkader R, Kawakami S, Unga J, Suzuki R, Maruyama K, Yamashita F, Hashida M. Evaluation of the potential of doxorubicin loaded microbubbles as a theranostic modality using a murine tumor model. Acta Biomater 2015; 19:112-8.

Andreano A, Laeseke P, Lava M, Zimbaro F, Daniela V, Meloni MF. Asymptomatic metastatic melanoma of the gallbladder diagnosed with contrast-enhanced ultrasonography. J Ultrasound Med 2010; 29:1133-7.

Averkiou MA, Bruce MF, Powers JE, Sheeran PS, Burns PN. Imaging Methods for Ultrasound Contrast Agents. Ultrasound Med Biol 2020; 46:498-517.

Backman H. Metastases of malignant melanoma in the gastrointestinal tract. Geriatrics 1969; 24:112-20.

Baghirov H, Snipstad S, Sulheim E, Berg S, Hansen R, Thorsen F, Morch Y, Davies CL, Aslund AKO. Ultrasound-mediated delivery and distribution of polymeric nanoparticles in the normal brain parenchyma of a metastatic brain tumour model. PLoS One 2018; 13:e0191102.

Barat M, Guegan-Bart S, Cottereau AS, Guillo E, Hoeffel C, Barret M, Gaujoux S, Dohan A, Soyer P. CT, MRI and PET/CT features of abdominal manifestations of cutaneous melanoma: a review of current concepts in the era of tumor-specific therapies. Abdom Radiol (NY) 2021; 46:2219-35.

Barenholz Y. Doxil(R)--the first FDA-approved nano-drug: lessons learned. J Control Release 2012; 160:117-34.

Barretta ML, Catalano O, Setola SV, Granata V, Marone U, D'Errico Gallipoli A. Gallbladder metastasis: spectrum of imaging findings. Abdom Imaging 2011; 36:729-34.

Bertelsen C, King KG, Swanson M, Duddalwar V, Pepper JP. Contrast-Enhanced Ultrasound With Perflubutane for Sentinel Lymph Node Mapping in Cutaneous Melanoma: A Pilot Study. Laryngoscope 2019; 129:1117-22.

Bichakjian CK, Halpern AC, Johnson TM, Foote Hood A, Grichnik JM, Swetter SM, Tsao H, Barbosa VH, Chuang TY, Duvic M, Ho VC, Sober AJ, Beutner KR, Bhushan R, Smith Begolka W, American Academy of D. Guidelines of care for the management of primary cutaneous melanoma. American Academy of Dermatology. J Am Acad Dermatol 2011; 65:1032-47.

Cammarota T, Pinto F, Magliaro A, Sarno A. Current uses of diagnostic high-frequency US in dermatology. Eur J Radiol 1998; 27 Suppl 2:S215-23.

Carvalho C, Santos RX, Cardoso S, Correia S, Oliveira PJ, Santos MS, Moreira PI. Doxorubicin: the good, the bad and the ugly effect. Curr Med Chem 2009; 16:3267-85.

Catalano O. Critical analysis of the ultrasonographic criteria for diagnosing lymph node metastasis in patients with cutaneous melanoma: a systematic review. J Ultrasound Med 2011; 30:547-60.

Chang ST, Desser TS, Gayer G, Menias CO. Metastatic melanoma in the chest and abdomen: the great radiologic imitator. Semin Ultrasound CT MR 2014; 35:272-89.

Chapman BC, Gleisner A, Kwak JJ, Hosokawa P, Paniccia A, Merkow JS, Koo PJ, Gajdos C, Pearlman NW, McCarter MD, Kounalakis N. SPECT/CT Improves Detection of Metastatic Sentinel Lymph Nodes in Patients with Head and Neck Melanoma. Ann Surg Oncol 2016; 23:2652-7.

Chaput L, Laurent E, Pare A, Sallot A, Mourtada Y, Ossant F, Vaillant L, Patat F, Machet L. One-step surgical removal of cutaneous melanoma with surgical margins based on preoperative ultrasound measurement of the thickness of the melanoma. Eur J Dermatol 2018; 28:202-08.

Coran A, Di Maggio A, Rastrelli M, Alberioli E, Attar S, Ortolan P, Bortolanza C, Tosi A, Montesco MC, Bezzon E, Rossi CR, Stramare R. Core needle biopsy of soft tissue tumors, CEUS vs US guided: a pilot study. J Ultrasound 2015; 18:335-42.

Corvino A, Catalano O, Corvino F, Petrillo A. Rectal melanoma presenting as a solitary complex cystic liver lesion: role of contrast-specific low-MI real-time ultrasound imaging. J Ultrasound 2016; 19:135-9.

Corvino A, Corvino F, Catalano O, Sandomenico F, Petrillo A. The Tail and the String Sign: New Sonographic Features of Subcutaneous Melanoma Metastasis. Ultrasound Med Biol 2017; 43:370-74.

De Giorgi V, Gori A, Grazzini M, Rossari S, Marino G, D'Elia G, Crocetti E, Roselli G, Innocenti P, Dini M, Lotti T. Contrast-enhanced ultrasound: a filter role in AJCC stage I/II melanoma patients. Oncology 2010; 79:370-5.

De Marchi A, Brach del Prever EM, Linari A, Pozza S, Verga L, Albertini U, Forni M, Gino GC, Comandone A, Brach del Prever AM, Piana R, Faletti C. Accuracy of core-needle biopsy after contrast-enhanced ultrasound in soft-tissue tumours. Eur Radiol 2010; 20:2740-8.

Dewitte H, Van Lint S, Heirman C, Thielemans K, De Smedt SC, Breckpot K, Lentacker I. The potential of antigen and TriMix sonoporation using mRNA-loaded microbubbles for ultrasound-triggered cancer immunotherapy. J Control Release 2014; 194:28-36.

Dinnes J, Ferrante di Ruffano L, Takwoingi Y, Cheung ST, Nathan P, Matin RN, Chuchu N, Chan SA, Durack A, Bayliss SE, Gulati A, Patel L, Davenport C, Godfrey K, Subesinghe M, Traill Z, Deeks JJ, Williams HC, Cochrane Skin Cancer Diagnostic Test Accuracy G. Ultrasound, CT, MRI, or PET-CT for staging and re-staging of adults with cutaneous melanoma. Cochrane Database Syst Rev 2019; 7:CD012806.

Dowling J, McGregor SP, Williford P. Update on Current Treatment Recommendations for Primary Cutaneous Melanoma. Dermatol Clin 2019; 37:397-407.

Escoffre JM, Deckers R, Bos C, Moonen C. Bubble-Assisted Ultrasound: Application in Immunotherapy and Vaccination. Adv Exp Med Biol 2016; 880:243-61.

Escudier B, Lassau N, Angevin E, Soria JC, Chami L, Lamuraglia M, Zafarana E, Landreau V, Schwartz B, Brendel E, Armand JP, Robert C. Phase I trial of sorafenib in combination with IFN alpha-2a in patients with unresectable and/or metastatic renal cell carcinoma or malignant melanoma. Clin Cancer Res 2007; 13:1801-9.

Ferlay J, Colombet M, Soerjomataram I, Dyba T, Randi G, Bettio M, Gavin A, Visser O, Bray F. Cancer incidence and mortality patterns in Europe: Estimates for 40 countries and 25 major cancers in 2018. Eur J Cancer 2018; 103:356-87.

Ferrara KW, Merritt CR, Burns PN, Foster FS, Mattrey RF, Wickline SA. Evaluation of tumor angiogenesis with US: imaging, Doppler, and contrast agents. Acad Radiol 2000; 7:824-39.

Flaherty KT, Hamilton BK, Rosen MA, Amaravadi RK, Schuchter LM, Gallagher M, Chen H, Sehgal C, O'Dwyer PJ. Phase I/II Trial of Imatinib and Bevacizumab in Patients With Advanced Melanoma and Other Advanced Cancers. Oncologist 2015; 20:952-9.

Forsberg F, Dicker AP, Thakur ML, Rawool NM, Liu JB, Shi WT, Nazarian LN. Comparing contrast-enhanced ultrasound to immunohistochemical markers of angiogenesis in a human melanoma xenograft model: preliminary results. Ultrasound Med Biol 2002; 28:445-51.

Forsberg F, Ro RJ, Liu JB, Lipcan KJ, Potoczek M, Nazarian LN. Monitoring angiogenesis in human melanoma xenograft model using contrast-enhanced ultrasound imaging. Ultrason Imaging 2008; 30:237-46.

Forsberg F, Ro RJ, Marshall A, Liu JB, Chiou SY, Merton DA, Machado P, Dicker AP, Nazarian LN. The antiangiogenic effects of a vascular endothelial growth factor decoy receptor can be monitored in vivo using contrast-enhanced ultrasound imaging. Mol Imaging 2014; 13:1-9.

Frinking P, Segers T, Luan Y, Tranquart F. Three Decades of Ultrasound Contrast Agents: A Review of the Past, Present and Future Improvements. Ultrasound Med Biol 2020; 46:892-908.

Frinking PJ, Bouakaz A, Kirkhorn J, Ten Cate FJ, de Jong N. Ultrasound contrast imaging: current and new potential methods. Ultrasound Med Biol 2000; 26:965-75.

Gambichler T, Moussa G, Bahrenberg K, Vogt M, Ermert H, Weyhe D, Altmeyer P, Hoffmann K. Preoperative ultrasonic assessment of thin melanocytic skin lesions using a 100-MHz ultrasound transducer: a comparative study. Dermatol Surg 2007; 33:818-24.

Gao X, Nan Y, Yuan Y, Gong X, Sun Y, Zhou H, Zong Y, Zhang L, Yu M. Gasfilled ultrasound microbubbles enhance the immunoactivity of the HSP70MAGEA1 fusion protein against MAGEA1expressing tumours. Mol Med Rep 2018; 18:315-21.

Gauthier M, Leguerney I, Thalmensi J, Chebil M, Parisot S, Peronneau P, Roche A, Lassau N. Estimation of intra-operator variability in perfusion parameter measurements using DCE-US. World J Radiol 2011; 3:70-81.

Gauthier M, Tabarout F, Leguerney I, Polrot M, Pitre S, Peronneau P, Lassau N. Assessment of quantitative perfusion parameters by dynamic contrast-enhanced sonography using a deconvolution method: an in vitro and in vivo study. J Ultrasound Med 2012; 31:595-608.

Geers B, Lentacker I, Sanders NN, Demeester J, Meairs S, De Smedt SC. Self-assembled liposome-loaded microbubbles: The missing link for safe and efficient ultrasound triggered drug-delivery. J Control Release 2011; 152:249-56.

Gershenwald JE, Scolyer RA. Melanoma Staging: American Joint Committee on Cancer (AJCC) 8th Edition and Beyond. Ann Surg Oncol 2018; 25:2105-10.

Goldberg BB, Merton DA, Liu JB, Forsberg F, Zhang K, Thakur M, Schulz S, Schanche R, Murphy GF, Waldman SA. Contrast-enhanced ultrasound imaging of sentinel lymph nodes after peritumoral administration of Sonazoid in a melanoma tumor animal model. J Ultrasound Med 2011; 30:441-53.

Goldberg BB, Merton DA, Liu JB, Thakur M, Murphy GF, Needleman L, Tornes A, Forsberg F. Sentinel lymph nodes in a swine model with melanoma: contrast-enhanced lymphatic US. Radiology 2004; 230:727-34.

Heger M, van Golen RF, Broekgaarden M, Michel MC. The molecular basis for the pharmacokinetics and pharmacodynamics of curcumin and its metabolites in relation to cancer. Pharmacol Rev 2014; 66:222-307.

Holloway BJ, King DM. Ultrasound diagnosis of metastatic melanoma of the gallbladder. Br J Radiol 1997; 70:1122-5.

Hu Y, Xue S, Long T, Lyu P, Zhang X, Chen J, Chen S, Liu C, Chen X. Opto-acoustic synergistic irradiation for vaporization of natural melanin-cored nanodroplets at safe energy levels and efficient sono-chemo-photothermal cancer therapy. Theranostics 2020; 10:10448-65.

Karimkhani C, Green AC, Nijsten T, Weinstock MA, Dellavalle RP, Naghavi M, Fitzmaurice C. The global burden of melanoma: results from the Global Burden of Disease Study 2015. Br J Dermatol 2017; 177:134-40.

Katz SC, Bowne WB, Wolchok JD, Busam KJ, Jaques DP, Coit DG. Surgical management of melanoma of the gallbladder: a report of 13 cases and review of the literature. Am J Surg 2007; 193:493-7.

Klibanov AL. Ultrasound Molecular Imaging of Cancer: Design and Formulation Strategies of Targeted Contrast Agents. Recent Results Cancer Res 2020; 216:319-36.

Kooiman K, Roovers S, Langeveld SAG, Kleven RT, Dewitte H, O'Reilly MA, Escoffre JM, Bouakaz A, Verweij MD, Hynynen K, Lentacker I, Stride E, Holland CK. Ultrasound-Responsive Cavitation Nuclei for Therapy and Drug Delivery. Ultrasound Med Biol 2020; 46:1296-325.

Lassau N, Bonastre J, Kind M, Vilgrain V, Lacroix J, Cuinet M, Taieb S, Aziza R, Sarran A, Labbe-Devilliers C, Gallix B, Lucidarme O, Ptak Y, Rocher L, Caquot LM, Chagnon S, Marion D, Luciani A, Feutray S, Uzan-Augui J, Coiffier B, Benastou B, Koscielny S. Validation of dynamic contrast-enhanced ultrasound in predicting outcomes of antiangiogenic therapy for solid tumors: the French multicenter support for innovative and expensive techniques study. Invest Radiol 2014; 49:794-800.

Lassau N, Chami L, Benatsou B, Peronneau P, Roche A. Dynamic contrast-enhanced ultrasonography (DCE-US) with quantification of tumor perfusion: a new diagnostic tool to evaluate the early effects of antiangiogenic treatment. Eur Radiol 2007; 17 Suppl 6:F89-98.

Lassau N, Chebil M, Chami L, Bidault S, Girard E, Roche A. Dynamic contrast-enhanced ultrasonography (DCE-US): a new tool for the early evaluation of antiangiogenic treatment. Target Oncol 2010; 5:53-8.

Lassau N, Koscielny S, Avril MF, Margulis A, Duvillard P, De Baere T, Roche A, Leclere J. Prognostic value of angiogenesis evaluated with high-frequency and color Doppler sonography for preoperative assessment of melanomas. AJR Am J Roentgenol 2002; 178:1547-51.

Lassau N, Lamuraglia M, Koscielny S, Spatz A, Roche A, Leclere J, Avril MF. Prognostic value of angiogenesis evaluated with high-frequency and colour Doppler sonography for preoperative assessment of primary cutaneous melanomas: correlation with recurrence after a 5 year follow-up period. Cancer Imaging 2006; 6:24-9.

Lavisse S, Lejeune P, Rouffiac V, Elie N, Bribes E, Demers B, Vrignaud P, Bissery MC, Brule A, Koscielny S, Peronneau P, Lassau N. Early quantitative evaluation of a tumor vasculature disruptive agent AVE8062 using dynamic contrast-enhanced ultrasonography. Invest Radiol 2008; 43:100-11.

Leguerney I, Lassau N, Koscielny S, Rodrigues M, Massard C, Rouffiac V, Benatsou B, Thalmensi J, Bawa O, Opolon P, Peronneau P, Roche A. Combining functional imaging and interstitial pressure measurements to evaluate two anti-angiogenic treatments. Invest New Drugs 2012; 30:144-56.

Leguerney I, Scoazec JY, Gadot N, Robin N, Penault-Llorca F, Victorin S, Lassau N. Molecular ultrasound imaging using contrast agents targeting endoglin, vascular endothelial growth factor receptor 2 and integrin. Ultrasound Med Biol 2015; 41:197-207.

Lekht I, Brauner N, Bakhsheshian J, Chang KE, Gulati M, Shiroishi MS, Grant EG, Christian E, Zada G. Versatile utilization of real-time intraoperative contrast-enhanced ultrasound in cranial neurosurgery: technical note and retrospective case series. Neurosurg Focus 2016; 40:E6.

Lentacker I, Geers B, Demeester J, De Smedt SC, Sanders NN. Design and evaluation of doxorubicin-containing microbubbles for ultrasound-triggered doxorubicin delivery: cytotoxicity and mechanisms involved. Mol Ther 2010; 18:101-8.

Li X, Lovell JF, Yoon J, Chen X. Clinical development and potential of photothermal and photodynamic therapies for cancer. Nat Rev Clin Oncol 2020; 17:657-74.

Liu JB, Merton DA, Berger AC, Forsberg F, Witkiewicz A, Zhao H, Eisenbrey JR, Fox TB, Goldberg BB. Contrast-enhanced sonography for detection of secondary lymph nodes in a melanoma tumor animal model. J Ultrasound Med 2014; 33:939-47.

Liu M, Zhang P, Deng L, Guo D, Tan M, Huang J, Luo Y, Cao Y, Wang Z. IR780-based light-responsive nanocomplexes combining phase transition for enhancing multimodal imaging-guided photothermal therapy. Biomater Sci 2019; 7:1132-46.

Lu Q, Zhang XL, Han H, Huang BJ, Ding H, Wang WP. Value of Perfusion Parameters for Differentiating Hepatocellular Carcinoma and Liver Metastasis With Hypervascularity and a Normal Hepatic Background on Contrast-Enhanced Ultrasound Imaging. J Ultrasound Med 2019; 38:2601-08.

Machet L, Belot V, Naouri M, Boka M, Mourtada Y, Giraudeau B, Laure B, Perrinaud A, Machet MC, Vaillant L. Preoperative measurement of thickness of cutaneous melanoma using high-resolution 20 MHz ultrasound imaging: A monocenter prospective study and systematic review of the literature. Ultrasound Med Biol 2009; 35:1411-20.

Matsuo M, Yamaguchi K, Feril LB, Jr., Endo H, Ogawa K, Tachibana K, Nakayama J. Synergistic inhibition of malignant melanoma proliferation by melphalan combined with ultrasound and microbubbles. Ultrason Sonochem 2011; 18:1218-24.

Molinari F, Meiburger KM, Giustetto P, Rizzitelli S, Boffa C, Castano M, Terreno E. Quantitative assessment of cancer vascular architecture by skeletonization of high-resolution 3-D contrast-enhanced ultrasound images: role of liposomes and microbubbles. Technol Cancer Res Treat 2014; 13:541-50.

Murphy-Lavallee J, Jang HJ, Kim TK, Burns PN, Wilson SR. Are metastases really hypovascular in the arterial phase? The perspective based on contrast-enhanced ultrasonography. J Ultrasound Med 2007; 26:1545-56.

Nam K, Stanczak M, Forsberg F, Liu JB, Eisenbrey JR, Solomides CC, Lyshchik A. Sentinel Lymph Node Characterization with a Dual-Targeted Molecular Ultrasound Contrast Agent. Mol Imaging Biol 2018; 20:221-29.

Nam K, Stapp R, Liu JB, Stanczak M, Forsberg F, O'Kane PL, Lin Z, Zhu Z, Li J, Solomides CC, Eisenbrey JR, Lyshchik A. Performance of Molecular Lymphosonography for Detection and Quantification of Metastatic Involvement in Sentinel Lymph Nodes. J Ultrasound Med 2019; 38:2103-10.

Nielsen KR, Klyver H, Chakera AH, Nedergaard L, Hesse B, Nielsen MB. Sentinel node detection in melanomas using contrast-enhanced ultrasound. Acta Radiol 2009; 50:412-17.

O'Brien ME, Wigler N, Inbar M, Rosso R, Grischke E, Santoro A, Catane R, Kieback DG, Tomczak P, Ackland SP, Orlandi F, Mellars L, Alland L, Tendler C, Group CBCS. Reduced cardiotoxicity and comparable efficacy in a phase III trial of pegylated liposomal doxorubicin HCl (CAELYX/Doxil) versus conventional doxorubicin for first-line treatment of metastatic breast cancer. Ann Oncol 2004; 15:440-9.

Oda Y, Suzuki R, Otake S, Nishiie N, Hirata K, Koshima R, Nomura T, Utoguchi N, Kudo N, Tachibana K, Maruyama K. Prophylactic immunization with Bubble liposomes and ultrasound-treated dendritic cells provided a four-fold decrease in the frequency of melanoma lung metastasis. J Control Release 2012; 160:362-6.

Pitre-Champagnat S, Leguerney I, Bosq J, Peronneau P, Kiessling F, Calmels L, Coulot J, Lassau N. Dynamic contrast-enhanced ultrasound parametric maps to evaluate intratumoral vascularization. Invest Radiol 2015; 50:212-7.

Prada F, Perin A, Martegani A, Aiani L, Solbiati L, Lamperti M, Casali C, Legnani F, Mattei L, Saladino A, Saini M, DiMeco F. Intraoperative contrast-enhanced ultrasound for brain tumor surgery. Neurosurgery 2014; 74:542-52; discussion 52.

Prasad C, Banerjee R. Ultrasound-Triggered Spatiotemporal Delivery of Topotecan and Curcumin as Combination Therapy for Cancer. J Pharmacol Exp Ther 2019; 370:876-93.

Prasad C, Bhatia E, Banerjee R. Curcumin Encapsulated Lecithin Nanoemulsions: An Oral Platform for Ultrasound Mediated Spatiotemporal Delivery of Curcumin to the Tumor. Sci Rep 2020; 10:8587.

Presset A, Bonneau C, Kazuyoshi S, Nadal-Desbarats L, Mitsuyoshi T, Bouakaz A, Kudo N, Escoffre JM, Sasaki N. Endothelial Cells, First Target of Drug Delivery Using Microbubble-Assisted Ultrasound. Ultrasound Med Biol 2020; 46:1565-83.

Punjabi SP, Blomley MJ, Cosgrove D, Teixeira F, Chu AC. Microbubble ultrasound: how can it help detect melanoma metastasis? Int J Dermatol 2006; 45:1004-6.

Quaia E, Calliada F, Bertolotto M, Rossi S, Garioni L, Rosa L, Pozzi-Mucelli R. Characterization of focal liver lesions with contrast-specific US modes and a sulfur hexafluoride-filled microbubble contrast agent: diagnostic performance and confidence. Radiology 2004; 232:420-30.

Ramalingam K, Allamaneni SS. Staging Melanoma: What's Old and New. Surg Clin North Am 2020; 100:29-41.
Rouffiac V, Duret JS, Peronneau P, Dehez N, Opolon P, Roche A, Lassau N. Combination of HIFU therapy with contrast-enhanced sonography for quantitative assessment of therapeutic efficiency on tumor grafted mice. Ultrasound Med Biol 2006; 32:729-40.
Rubaltelli L, Beltrame V, Scagliori E, Bezzon E, Frigo AC, Rastrelli M, Stramare R. Potential use of contrast-enhanced ultrasound (CEUS) in the detection of metastatic superficial lymph nodes in melanoma patients. Ultraschall Med 2014; 35:67-71.
Rubaltelli L, Beltrame V, Tregnaghi A, Scagliori E, Frigo AC, Stramare R. Contrast-enhanced ultrasound for characterizing lymph nodes with focal cortical thickening in patients with cutaneous melanoma. AJR Am J Roentgenol 2011; 196:W8-12.
Sarkisian S, Nair S, Sharma R. Current Clinical Trials in the Treatment of Advanced Melanomas. Surg Clin North Am 2020; 100:201-08.
Schmid-Wendtner MH, Partscht K, Korting HC, Volkenandt M. Improved differentiation of benign and malignant lymphadenopathy in patients with cutaneous melanoma by contrast-enhanced color Doppler sonography. Arch Dermatol 2002; 138:491-7.
Schroeder RJ, Hauff P, Bartels T, Vogel K, Jeschke J, Hidajat N, Maeurer J. Tumor vascularization in experimental melanomas: correlation between unenhanced and contrast enhanced power Doppler imaging and histological grading. Ultrasound Med Biol 2001; 27:761-71.
Schroer-Gunther MA, Wolff RF, Westwood ME, Scheibler FJ, Schurmann C, Baumert BG, Sauerland S, Kleijnen J. F-18-fluoro-2-deoxyglucose positron emission tomography (PET) and PET/computed tomography imaging in primary staging of patients with malignant melanoma: a systematic review. Syst Rev 2012; 1:62.
Seiler GS, Ziemer LS, Schultz S, Lee WM, Sehgal CM. Dose-response relationship of ultrasound contrast agent in an in vivo murine melanoma model. Cancer Imaging 2007; 7:216-23.
Sennoga CA, Kanbar E, Auboire L, Dujardin PA, Fouan D, Escoffre JM, Bouakaz A. Microbubble-mediated ultrasound drug-delivery and therapeutic monitoring. Expert Opin Drug Deliv 2017; 14:1031-43.
Serrone L, Solivetti FM, Thorel MF, Eibenschutz L, Donati P, Catricala C. High frequency ultrasound in the preoperative staging of primary melanoma: a statistical analysis. Melanoma Res 2002; 12:287-90.
Slingluff CL, Jr., Petroni GR, Olson W, Czarkowski A, Grosh WW, Smolkin M, Chianese-Bullock KA, Neese PY, Deacon DH, Nail C, Merrill P, Fink R, Patterson JW, Rehm PK. Helper T-cell responses and clinical activity of a melanoma vaccine with multiple peptides from MAGE and melanocytic differentiation antigens. J Clin Oncol 2008; 26:4973-80.
Sofue K, Tateishi U, Tsurusaki M, Arai Y, Yamazaki N, Sugimura K. MR imaging of hepatic metastasis in patients with malignant melanoma: evaluation of suspected lesions screened at contrast-enhanced CT. Eur J Radiol 2012; 81:714-8.
Sonoda S, Tachibana K, Uchino E, Yamashita T, Sakoda K, Sonoda KH, Hisatomi T, Izumi Y, Sakamoto T. Inhibition of melanoma by ultrasound-microbubble-aided drug delivery suggests membrane permeabilization. Cancer Biol Ther 2007; 6:1276-83.
Suzuki R, Namai E, Oda Y, Nishiie N, Otake S, Koshima R, Hirata K, Taira Y, Utoguchi N, Negishi Y, Nakagawa S, Maruyama K. Cancer gene therapy by IL-12 gene delivery using liposomal bubbles and tumoral ultrasound exposure. J Control Release 2010; 142:245-50.
Tardelli E, Mazzarri S, Rubello D, Gennaro M, Fantechi L, Duce V, Romanini A, Chondrogiannis S, Volterrani D, Colletti PM, Manca G. Sentinel Lymph Node Biopsy

in Cutaneous Melanoma: Standard and New Technical Procedures and Clinical Advances. A Systematic Review of the Literature. Clin Nucl Med 2016; 41:e498-e507.
Tartis MS, McCallan J, Lum AF, LaBell R, Stieger SM, Matsunaga TO, Ferrara KW. Therapeutic effects of paclitaxel-containing ultrasound contrast agents. Ultrasound Med Biol 2006; 32:1771-80.
Un K, Kawakami S, Suzuki R, Maruyama K, Yamashita F, Hashida M. Development of an ultrasound-responsive and mannose-modified gene carrier for DNA vaccine therapy. Biomaterials 2010; 31:7813-26.
Un K, Kawakami S, Suzuki R, Maruyama K, Yamashita F, Hashida M. Suppression of melanoma growth and metastasis by DNA vaccination using an ultrasound-responsive and mannose-modified gene carrier. Mol Pharm 2011; 8:543-54.
Un K, Kono Y, Yoshida M, Yamashita F, Kawakami S, Hashida M. Enhancement of gene expression by transcriptional activation using doxorubicin-loaded liposome/pDNA complexes. Pharmazie 2012; 67:400-5.
Ungureanu L, Botar Jid C, Candrea E, Cosgarea R, Senila SC. The role of lymph node ultrasound evaluation in melanoma - review of the literature. Med Ultrason 2016; 18:224-30.
Velazquez HE, Castro-Alonso FJ, Bourlon C, Gabutti A, Gallegos C, Bourlon MT. Diffuse Hepatic Infiltration by Metastatic Melanoma. Oncology (Williston Park) 2019; 33.
Voit C, Van Akkooi AC, Schafer-Hesterberg G, Schoengen A, Kowalczyk K, Roewert JC, Sterry W, Eggermont AM. Ultrasound morphology criteria predict metastatic disease of the sentinel nodes in patients with melanoma. J Clin Oncol 2010; 28:847-52.
Wang YH, Chen SP, Liao AH, Yang YC, Lee CR, Wu CH, Wu PC, Liu TM, Wang CR, Li PC. Synergistic delivery of gold nanorods using multifunctional microbubbles for enhanced plasmonic photothermal therapy. Sci Rep 2014; 4:5685.
Wildner D, Schellhaas B, Strack D, Goertz RS, Pfeifer L, Fiessler C, Neurath MF, Strobel D. Differentiation of malignant liver tumors by software-based perfusion quantification with dynamic contrast-enhanced ultrasound (DCEUS). Clin Hemorheol Microcirc 2019; 71:39-51.
Wood AK, Bunte RM, Schultz SM, Sehgal CM. Acute increases in murine tumor echogenicity after antivascular ultrasound therapy: a pilot preclinical study. J Ultrasound Med 2009; 28:795-800.
Xu F, Zhu J, Lin L, Zhang C, Sun W, Fan Y, Yin F, van Hest JCM, Wang H, Du L, Shi X. Multifunctional PVCL nanogels with redox-responsiveness enable enhanced MR imaging and ultrasound-promoted tumor chemotherapy. Theranostics 2020; 10:4349-58.
Yamaguchi K, Feril LB, Jr., Tachibana K, Takahashi A, Matsuo M, Endo H, Harada Y, Nakayama J. Ultrasound-mediated interferon beta gene transfection inhibits growth of malignant melanoma. Biochem Biophys Res Commun 2011; 411:137-42.
Zolochevska O, Xia X, Williams BJ, Ramsay A, Li S, Figueiredo ML. Sonoporation delivery of interleukin-27 gene therapy efficiently reduces prostate tumor cell growth in vivo. Hum Gene Ther 2011; 22:1537-50.

FIGURE LEGENDS

Figure 1. Flowchart of publication selection.

Figure 2. CEUS of murine melanoma. To get this original data, B16F10 cells (1×10^6 cells in 100 µL of phosphate-buffered saline) were subcutaneously injected in the left flank of a C57Bl6 mouse under gaseous anesthesia. CEUS was performed on the 7th day of the tumor growth. A bolus injection of 70 µL of Vevo Micromarkers UCAs (VisualSonics Inc., Toronto, Canada) was intravenously performed. Immediately afterward, a first set of nonlinear contrast images was acquired at low transmitted power. A 65 s video clip was recorded at 10 frame/s to assess the tumor perfusion (A-D). After image acquisition, quantitative analysis of the tumor perfusion was performed using VevoCQ software (VisualSonics Inc.). Motion artifacts were corrected, and a region of interest (green solid line) corresponding to the melanoma was manually defined. A time–intensity curve for this region was then computed (E). Images A to D were indicated on the time–intensity curve. The Animal Care and Regional Committee for Ethics in Animal Experiments, Centre Val de Loire approved all this procedure (N°2019091911211270).

Figure 3. Expression levels of endoglin, $\alpha v\beta_3$ integrin and VEGFR2 using US molecular imaging in murine melanoma models. (a) Time-intensity curves obtained for the four random bolus injections of UCAs (IgG control UCAs, endoglin-targeted UCAs, VEGFR2-targeted UCAs and $\alpha v\beta_3$ integrin-targeted UCAs) on the same animal from the control group at baseline. (b-e) Differential targeted enhancement with the corresponding region of interest (ROI) on both B-mode and harmonic images obtained from VEVO 2100 onboard software. The mean signal is represented before and after UCA destruction, with the burst destruction as a vertical line. IgG control UCAs (b) exhibit no difference in signal intensity between pre- and post-destruction

of UCAs compared to endoglin-targeted UCAs (c), VEGFR2-targeted UCAs (d) and $\alpha_v\beta_3$ integrin-targeted UCAs (e). Adapted with permission from Leguerney et al., (2015). Copyright 2015, World Federation for Ultrasound in Medicine & Biology. Published by Elsevier B.V.

Figure 4. CEUS of cutaneous melanoma and its SLNs in swine melanoma model. (A) Grayscale US (left) and CEUS (right) images of cutaneous melanoma of right posterior neck (long arrows) with injected Sonazoid UCAs seen in the adjacent tissues (short arrows). (B) Enhancing SLN (arrows) associated with the same tumor shown *in-vivo*. (C) Enhancing SLN (arrows) associated with this tumor scanned *ex-vivo*. Adapted with permission from Bertelsen et al., (2019). Copyright 2018 The American Laryngological, Rhinological and Otological Society, Inc.

Figure 5. CEUS of metastatic melanoma of the gallbladder in patient. (A) Grayscale sonogram showing a heterogeneous mass isoechoic to the liver that occupies the gallbladder fundus. (B) Contrast-enhanced sonogram, arterial phase. After administration of SonoVue UCAs, the tumor shows enhancement in the arterial phase (right panel, arrow). (C) Contrast-enhanced sonogram, portal phase. The mass shows early rapid washout (right panel). (D) Contrast-enhanced sonogram, late phase. The tumor wash-out is more evident in this later image (right panel). The left panels in B-D are grayscale images at a low mechanical index used as anatomic references for the corresponding images showing the signal from the contrast agent (right panels). Adapted with permission from Andreano et al., (2010). Copyright 2010 The American Institute of Ultrasound in Medicine.

Figure 6. Evaluation of DOX-loaded MBs (DLMBs) for an acoustically mediated drug delivery in mouse melanoma model. (A-C) Doxorubicin (DOX) distribution characteristics after i.v. administration of DLMBs with or without US in melanoma tumor bearing mice. The DOX content was measured in (A) tumor, (B) heart and (C) liver. Each bar represents the mean ± SEM of five experiments. *$P < 0.05$ *versus* the corresponding group that received DLMBs in

combination with US exposure. (D-E) Tumor inhibition study. (D) Tumor volume in mice. (E) Mouse body weight. Mice were divided into three groups: control (N.T.); DLMBs only (DLMBs-US); and DLMBs in combination with US exposure (DLMBs+US). Treatment was performed on the 9^{th} day after tumor transplantation and was repeated on the 11^{th} and 13^{th} days. Each bar represents the mean ± SEM of 5-6 experiments. *P < 0.05. Adapted with permission from Abdalkader et al., (2015).

Figure 7. Reduction of B16/BL6 lung metastasis following immunization with B16BL6 treated DCs. DCs were treated with B16/BL6-extracted Ags and cultured *in-vitro*. C57BL/6 mice were immunized with the DCs twice with a one-week interval. One week after the second immunization, B16/BL6 cells were injected into the tail vein; after another two weeks, animals were sacrificed and lungs assessed for metastases. (A) Counts of lung metastatic colonies (mean ± SD; n=6). *P < 0.05 (ANOVA, comparing all DC-immunized groups). (B) Images of lung by stereomicroscope. Adapted with permission from Oda et al., (2012).

Table 1. Inclusion and exclusion criteria used to select studies

Inclusion criteria	**Exclusion criteria**
Involving microbubble-assisted ultrasound	Ultrasound without microbubbles
Concerning melanoma skin cancer	Review papers, comments, Letters
Studies investigating the use of microbubble-mediated ultrasound for the imaging of melanoma	Other languages
Studies investigating the use of microbubble-mediated ultrasound for the treatment of melanoma	
In-vitro, animals and patients	
English	

Table 2. CEUS of melanoma in clinics

References	Application	Number of patients	Microbubbles (type, concentration/volume, administration way)	Main outcomes
(Schmid-Wendtner, et al. 2002)	Detection of metastases in LNs	19	▪ Levovist UCAs ▪ i.v. injection ▪ 8 mL at 312.5 mg/mL	▪ Help to differentiate LN metastases from reactive LNs, hematomas or seromas
(Nielsen, et al. 2009)	Detection of metastases in LNs	10	▪ SonoVue UCAs ▪ s.c. injection ▪ 1 mL at 8 or 16 µL/mL	▪ Detection of 2 contrast-enhanced inguinal LNs in one patient only
(De Giorgi, et al. 2010)	Detection of metastases in LNs	15	▪ SonoVue UCAs ▪ i.v. injection ▪ 2.4 mL followed by a bolus injection of saline solution (10 mL)	▪ Sensitivity: 100% ▪ Specificity: 61.5% ▪ PPV: 54.5% ▪ NPV: 100%
(Rubaltelli, et al. 2011)	Detection of metastases in LNs	436	▪ SonoVue UCAs ▪ i.v. injection ▪ 4.8 mL followed by a bolus injection of saline solution (10 mL)	▪ Sensitivity: 100% ▪ Specificity: 99.5% ▪ PPV: 86.7% ▪ NPV: 100%
(Rubaltelli, et al. 2014)	Detection of metastases in LNs	540	▪ SonoVue UCAs ▪ i.v. injection ▪ 4.8 mL followed by a bolus injection of saline solution (20 mL)	▪ Sensitivity: 98% ▪ Specificity: 99% ▪ Accuracy: 99%
(Punjabi, et al. 2006)	Detection of metastases in gall bladder	1	▪ SonoVue UCAs ▪ i.v. injection ▪ 2.4 mL	▪ Metastases are very well perfused
(Murphy-Lavallee, et al. 2007)	Detection of liver metastases	50 but only 3 with liver metastases from melanoma	▪ Definity UCAs ▪ i.v. injection ▪ 0.1 to 0.3 mL (standard dose, 0.2 mL) followed by a bolus injection of saline solution (5 mL)	▪ Metastases are hypervascular. A rapid and transient arterial contrast enhancement followed by a very rapid wash-out are observed
(Andreano, et al. 2010)	Detection of metastases in gall bladder	1	▪ SonoVue UCAs ▪ i.v. injection ▪ 2.4 mL followed by a bolus injection of saline solution (10 mL)	▪ Metastasis showed a rapid contrast enhancement a followed by a very rapid wash-out, which are characteristic of a malignant lesion
(Barretta, et al. 2011)	Detection of metastases in gall bladder	▪ 13 but 11 with cutaneous melanoma ▪ 8/11 investigated with CEUS	▪ SonoVue UCAs ▪ i.v. injection ▪ 2.4 mL followed by a bolus injection of saline solution (10 mL)	▪ Metastases showed a moderate to intense contrast enhancement in the arterial phase a followed by a more or less rapid wash-out in the venous phase
(Corvino, et al. 2016)	Detection of cystic hepatic metastases	1 with rectal melanoma	▪ SonoVue UCAs ▪ i.v. injection ▪ 2.4 mL followed by a bolus injection of saline solution (10 mL)	▪ Metastasis revealed a hyper-enhancement of the cystic wall and intracystic septation in the arterial phase

				followed by rapid wash-out in the portal and late phases
(Wildner, et al. 2019)	Detection of liver metastases	148 but only 7 with liver metastasis from melanoma	▪ SonoVue UCAs ▪ i.v. injection ▪ 1.5 mL followed by a bolus injection of saline solution (10 mL)	▪ Metastasis showed a rapid contrast enhancement a followed by a very rapid wash-out, which are characteristic of a malignant lesion
(Lekht, et al. 2016)	CEUS-guided surgery	1 patient with brain metastases from melanoma	▪ Definity UCAs ▪ i.v. injection ▪ 0.3 mL followed by a bolus injection of saline solution (10 mL)	▪ Metastases revealed an intense arterial contrast enhancement followed by delayed wash-out ▪ The real-time DCEUS evaluation helped to a maximal tumor resection without intraoperative complications
(Escudier, et al. 2007)	Monitoring of therapeutic follow-up (Sorafenib/IFN α-2a combination)	13 patients but only 1 with melanoma	▪ SonoVue UCAs ▪ i.v. injection ▪ 4.8 mL at 8 µL/mL	▪ Overall best response of stable disease was observed and confirmed for melanoma patient
(Lassau, et al. 2014)	Monitoring of therapeutic follow-up (anti-angiogenic treatment including Sorafenib, Bevacizumab, Sunitinib, Imatinib, *etc.*)	52 patients with metastatic melanoma	▪ SonoVue UCAs ▪ i.v. injection ▪ 4.8 mL followed by a bolus injection of saline solution (5 mL)	▪ DCEUS provide a predictive biomarker of tumor progression, termed as the change in AUC (a perfusion parameter linked to blood volume) from baseline to day 30 ▪ Patients with a greater than 40% decrease in AUC on day 30 revealed freedom from progression and overall survival

LNs, lymph nodes; i.v., intravenous; s.c., subcutaneous; NPV, negative prediction value; PPV, positive prediction value; DCEUS, dynamic contrast-enhanced ultrasound; AUC, area under the curve.

Table 3. Chemotherapy

References	Drug	Tumor model	Main outcomes

(Prasad and Banerjee 2019)	Curcumin, Topotecan	s.c. B16F10 melanoma mouse model	▪ Inhibition of tumor growth ▪ Increase in mouse survival
(Prasad, et al. 2020)	Curcumin	s.c. B16F10 melanoma mouse model	▪ Inhibition of tumor growth ▪ Increase in mouse survival
(Baghirov, et al. 2018)	Polymeric nanoparticles (without drugs)	H1_DL2 melanoma brain metastasis mouse model	▪ Increase in i.t. concentration of nanoparticles
(Geers, et al. 2011)	Doxorubicin	BLM melanoma cells	▪ Decrease in cell viability
(Lentacker, et al. 2010)	Doxorubicin	BLM melanoma cells	▪ Increase in intracellular concentration of doxorubicin ▪ Decrease in cell viability
(Abdalkader, et al. 2015)	Doxorubicin	s.c. B16BL6 melanoma mouse model	▪ Increase in i.t. concentration of doxorubicin ▪ Inhibition of tumor growth
(Xu, et al. 2020)	Doxorubicin	s.c. B16 melanoma cells	▪ Inhibition of tumor growth
(Sonoda, et al. 2007)	Bleomycin	s.c. B16 melanoma cells	▪ Inhibition of tumor growth
(Tartis, et al. 2006)	Paclitaxel	A375m melanoma cells	▪ Decrease in cell viability
(Matsuo, et al. 2011)	Melphalan	s.c. C32 melanoma mouse model	▪ Inhibition of tumor growth

s.c., subcutaneous tumor; i.t., intratumoral

Table 4. Photothermal therapy

References	Agent	Tumor model	Main outcomes
(Hu, et al. 2020)	Melanin (with Doxorubicin)	s.c. A375 melanoma mouse model	▪ Increase in i.t. concentration of melanin ▪ Inhibition of tumor growth
(Liu, et al. 2019)	IR780-based nanocomplex	s.c. B16 melanoma mouse model	▪ Increase in i.t. concentration of nanocomplex ▪ Inhibition of tumor growth
(Wang, et al. 2014)	Gold nanorods	s.c. B16F10 melanoma mouse model	▪ Increase in i.t. concentration of gold nanorods

s.c., subcutaneous tumor; i.t., intratumoral.

Table 5. Immunotherapy and Vaccination

References	Drug	Tumor model	Main outcomes
(Oda, et al. 2012)	Exogenous melanoma-associated Ags	B16/BL6 melanoma lung metastasis mouse model	▪ Induction of prophylactic immunization ▪ Reduction of lung metastases
(Gao, et al. 2018)	HSP70-MAGEA1 fusion protein	s.c. B16 melanoma mouse model	▪ Induction of cellular and humoral immune responses ▪ Inhibition of tumor growth ▪ Increase in mouse survival
(Dewitte, et al. 2014)	Immunodulating TriMix mRNA	s.c. MO4 melanoma mouse model	▪ Effective induction of Ag-specific T cells ▪ Induction of specific lysis of Ag-expressing cells ▪ Inhibition of tumor growth ▪ Induction of long-term Ag-specific immunological memory
(Yamaguchi, et al. 2011)	pDNA encoding interferon-β	s.c. C32 melanoma mouse model	▪ Inhibition of tumor growth
(Un, et al. 2010, Un, et al. 2011)	pDNA encoding gp100 and TRP-2	▪ s.c. B16/BL6 melanoma mouse model ▪ B16/BL6 melanoma lung metastasis mouse model	▪ Induction of prophylactic immunization ▪ Enhanced secretion of Th1 cytokines ▪ Enhanced activities of CTLs ▪ Inhibition of the growth of primary tumors ▪ Reduction of lung metastases
(Un, et al. 2012)	pDNA encoding gp100 and TRP-2 (in combination with Doxorubicin-encapsulated PEGylated liposomes)	▪ s.c. B16/BL6 melanoma mouse model ▪ B16/BL6 melanoma lung metastasis mouse model	▪ Enhanced activities of CTLs ▪ Inhibition of the growth of primary tumors ▪ Reduction of lung metastases ▪ Increase in mouse survival

s.c., subcutaneous tumor; i.t., intratumoral; Ag, antigen; mRNA, messenger RNA; HSP70, heat-shock protein 70; MAGEA1, melanoma-asso<ciated Ag-1; gp100, glycoprotein 100; TRP-2, Tyrosinase-related protein 2; pDNA, plasmid DNA; CTL, Cytotoxic T lymphocytes.

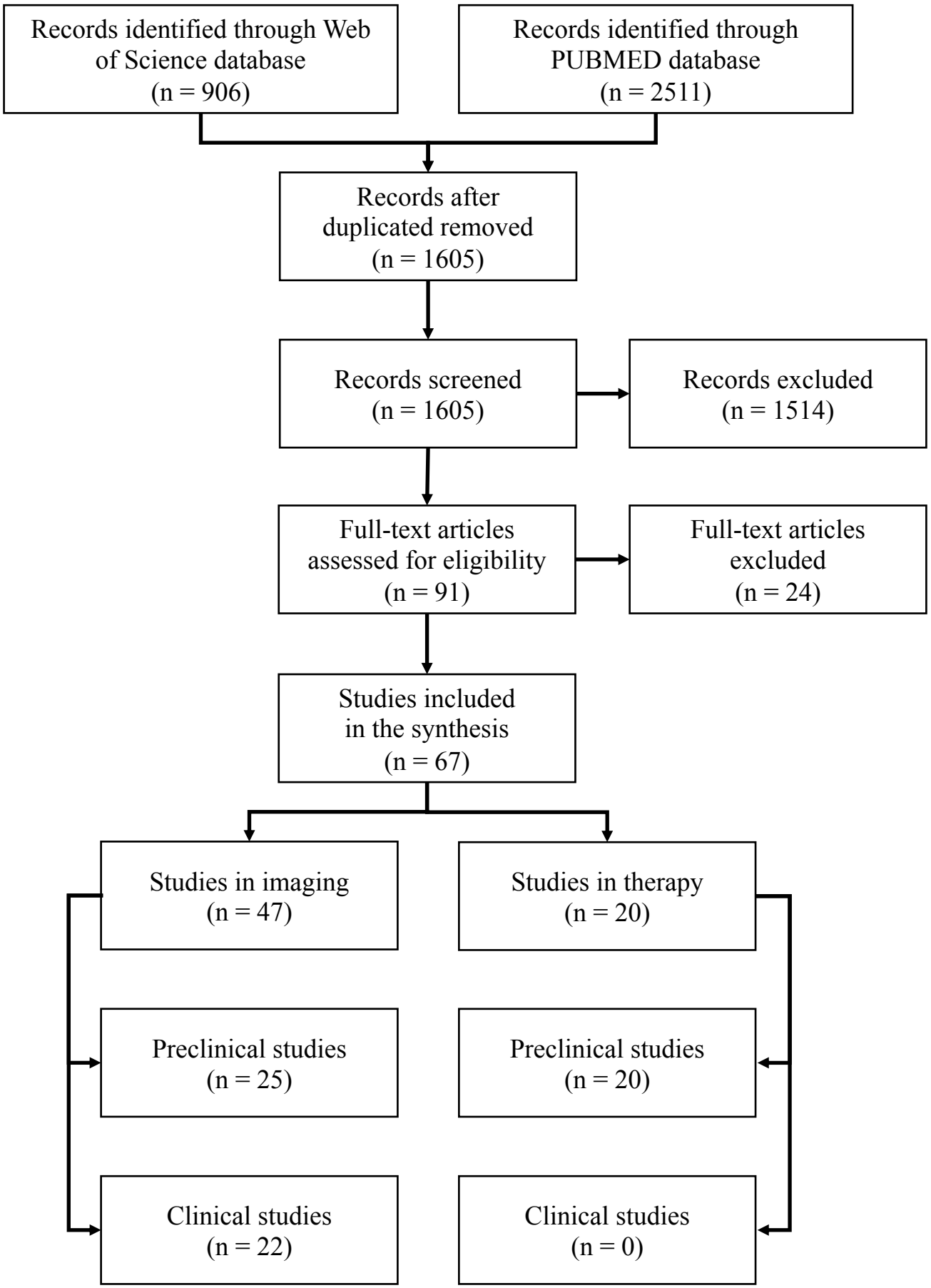
Records identified through Web of Science database (n = 906)
Records identified through PUBMED database (n = 2511)
Records after duplicated removed (n = 1605)
Records screened (n = 1605)
Records excluded (n = 1514)
Full-text articles assessed for eligibility (n = 91)
Full-text articles excluded (n = 24)
Studies included in the synthesis (n = 67)
Studies in imaging (n = 47)
Studies in therapy (n = 20)
Preclinical studies (n = 25)
Preclinical studies (n = 20)
Clinical studies (n = 22)
Clinical studies (n = 0)

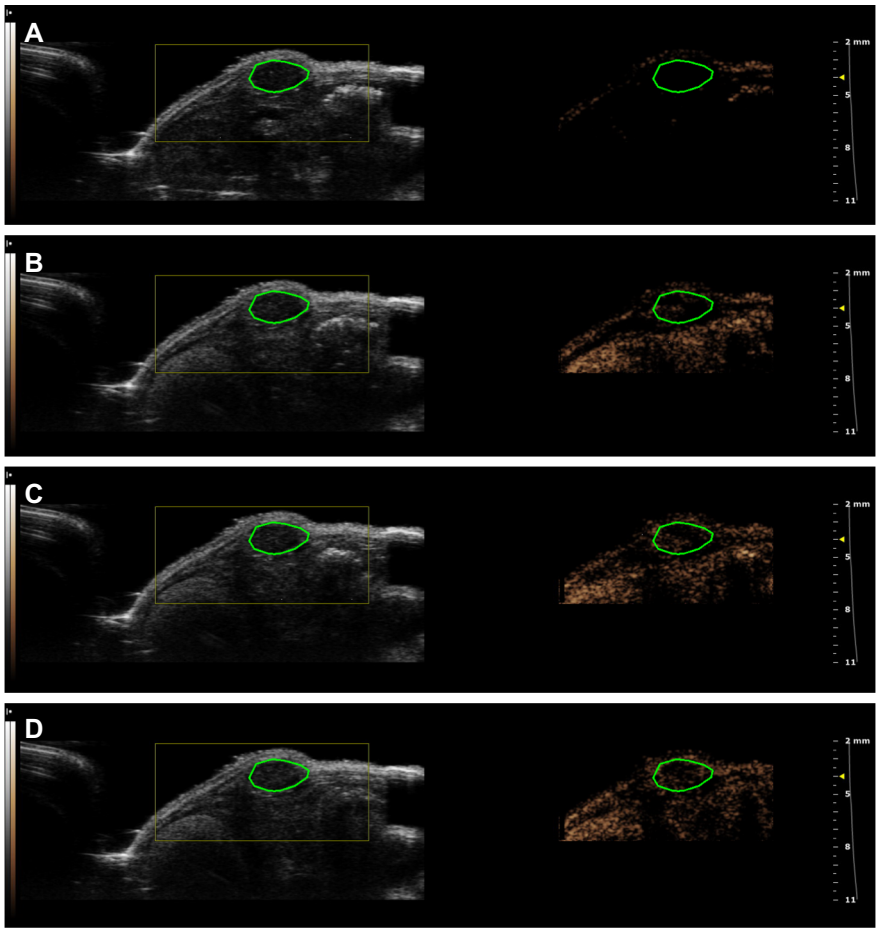
A
B
C
D

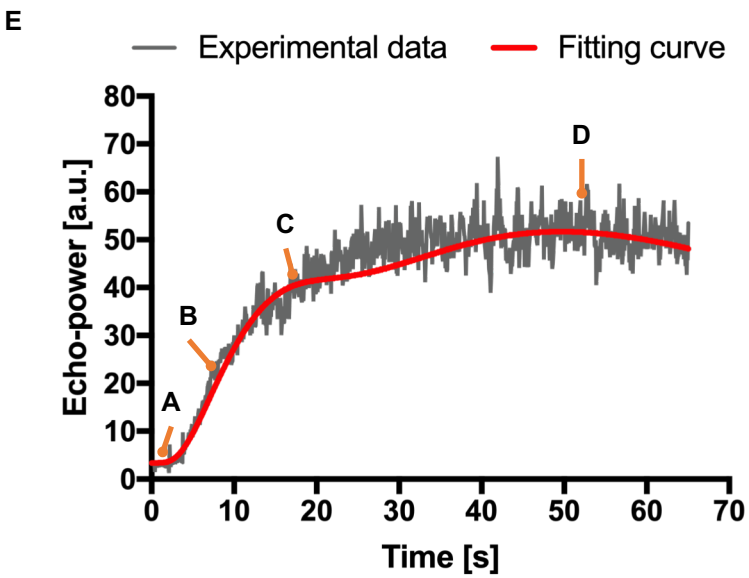
E
Experimental data
Fitting curve
Echo-power [a.u.]
Time [s]
A
B
C
D
0
10
20
30
40
50
60
70
80

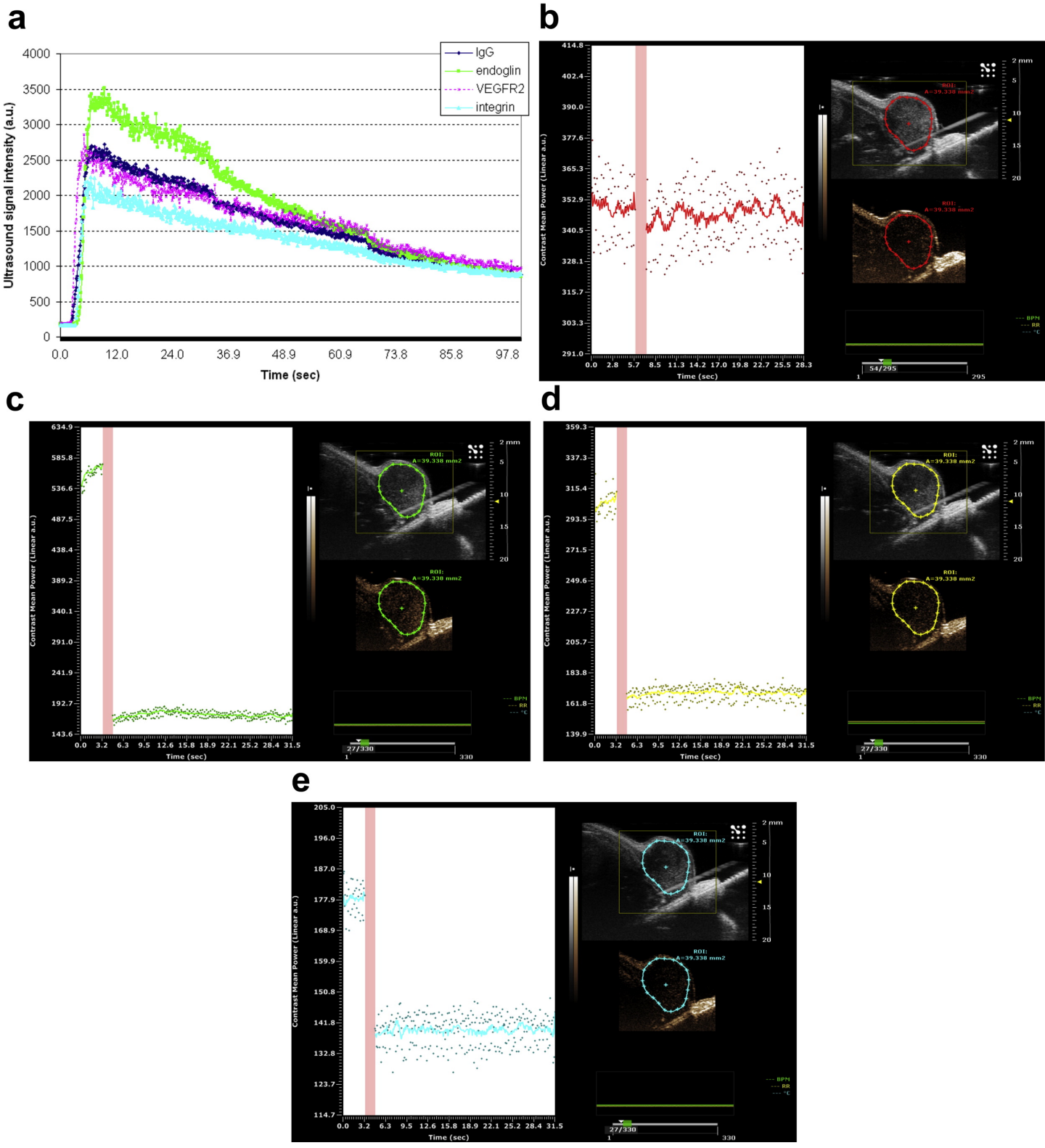
a
b
c
d
e
IgG
endoglin
VEGFR2
integrin
Ultrasound signal intensity (a.u.)
Time (sec)
Contrast Mean Power (Linear a.u.)
ROI:
A=39.338 mm2
2 mm
54/295
27/330
BPM
RR
°C

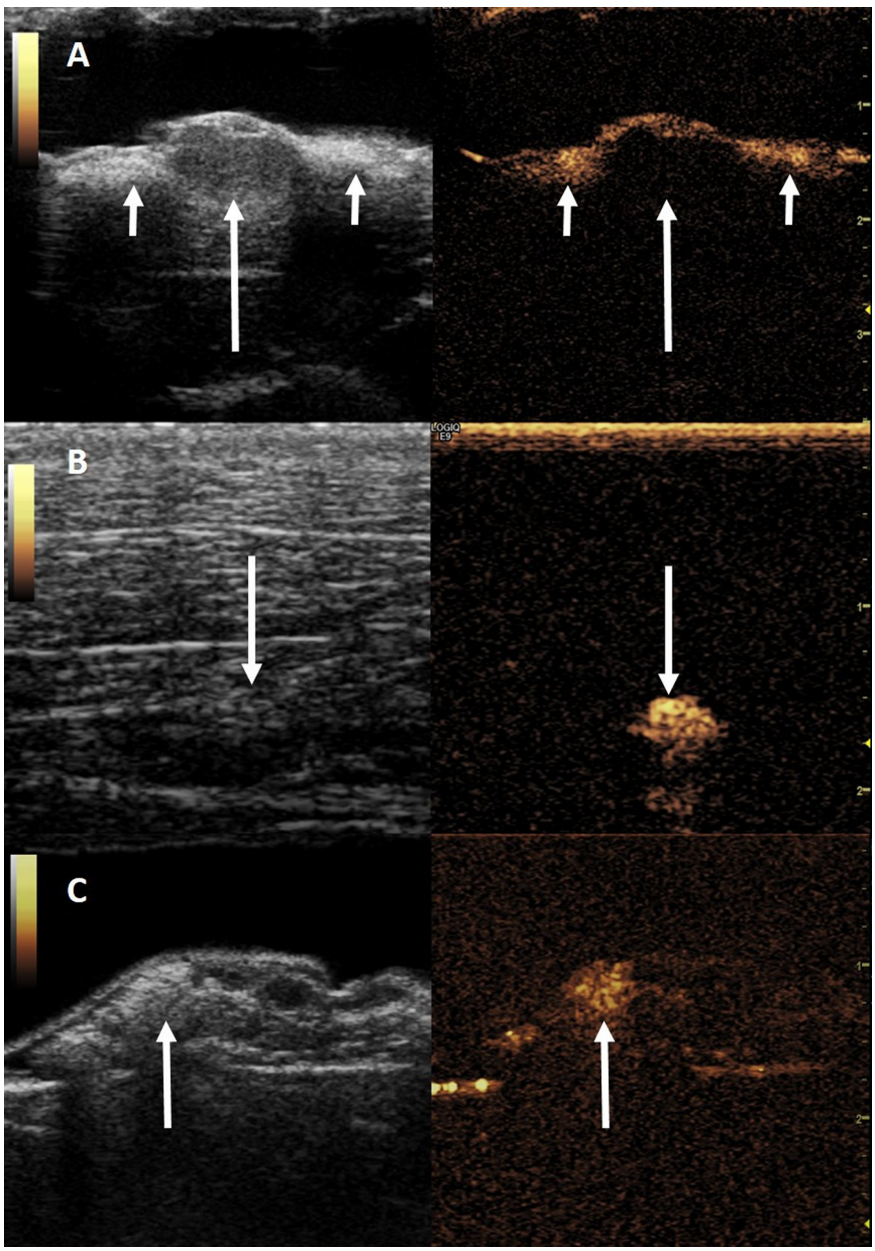
A
B
C

A

B

C

D

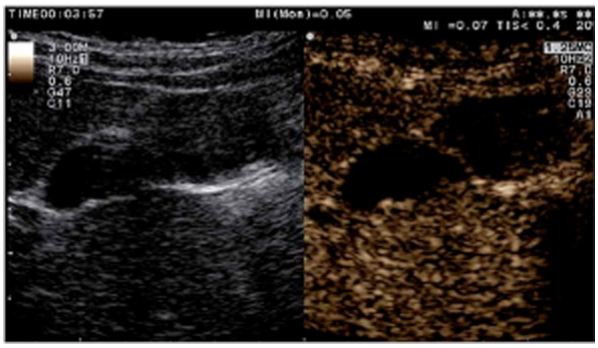

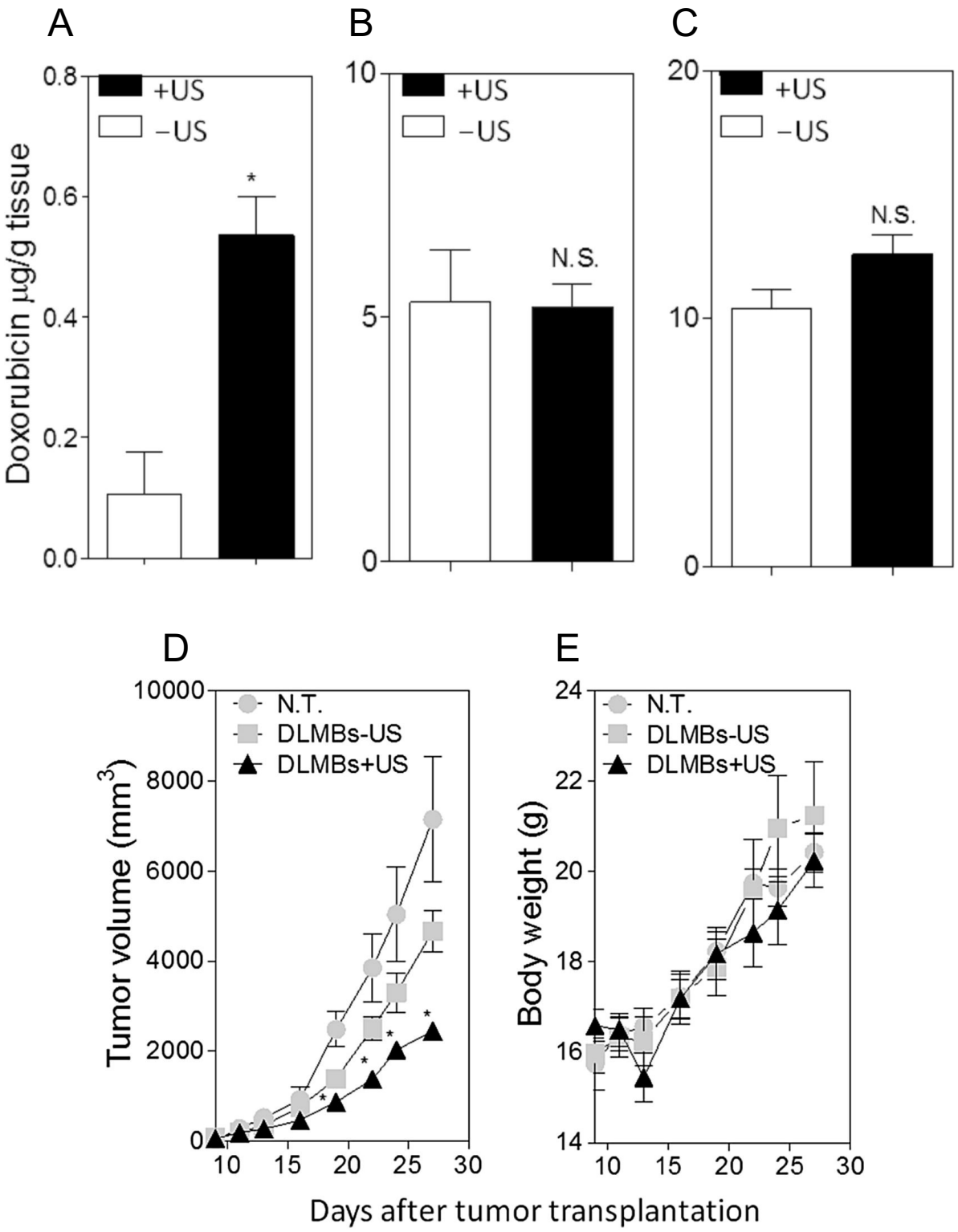
A
B
C
+US
−US
Doxorubicin μg/g tissue
0.8
0.6
0.4
0.2
0.0
*
10
5
0
N.S.
20
10
0
D
E
N.T.
DLMBs-US
DLMBs+US
Tumor volume (mm3)
10000
8000
6000
4000
2000
0
Body weight (g)
24
22
20
18
16
14
10
15
20
25
30
Days after tumor transplantation

A

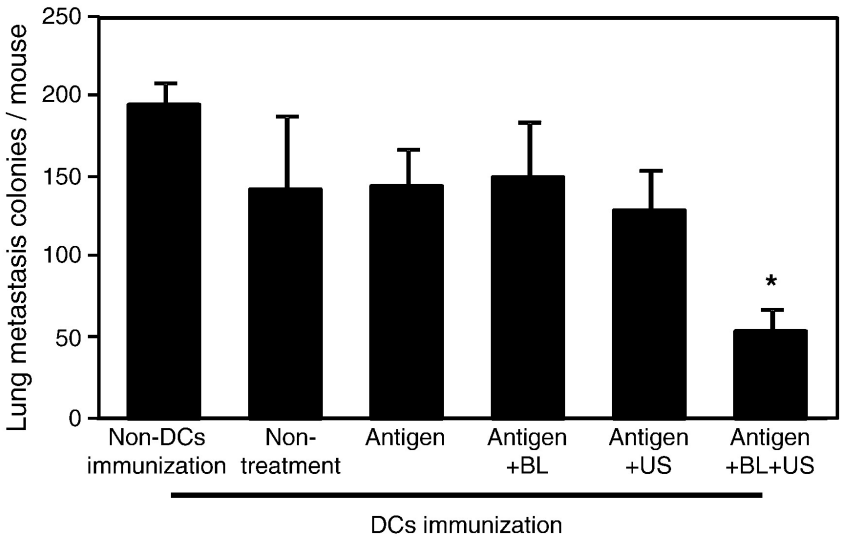
Lung metastasis colonies / mouse
250
200
150
100
50
0
*
Non-DCs immunization
Non-treatment
Antigen
Antigen +BL
Antigen +US
Antigen +BL+US
DCs immunization

B

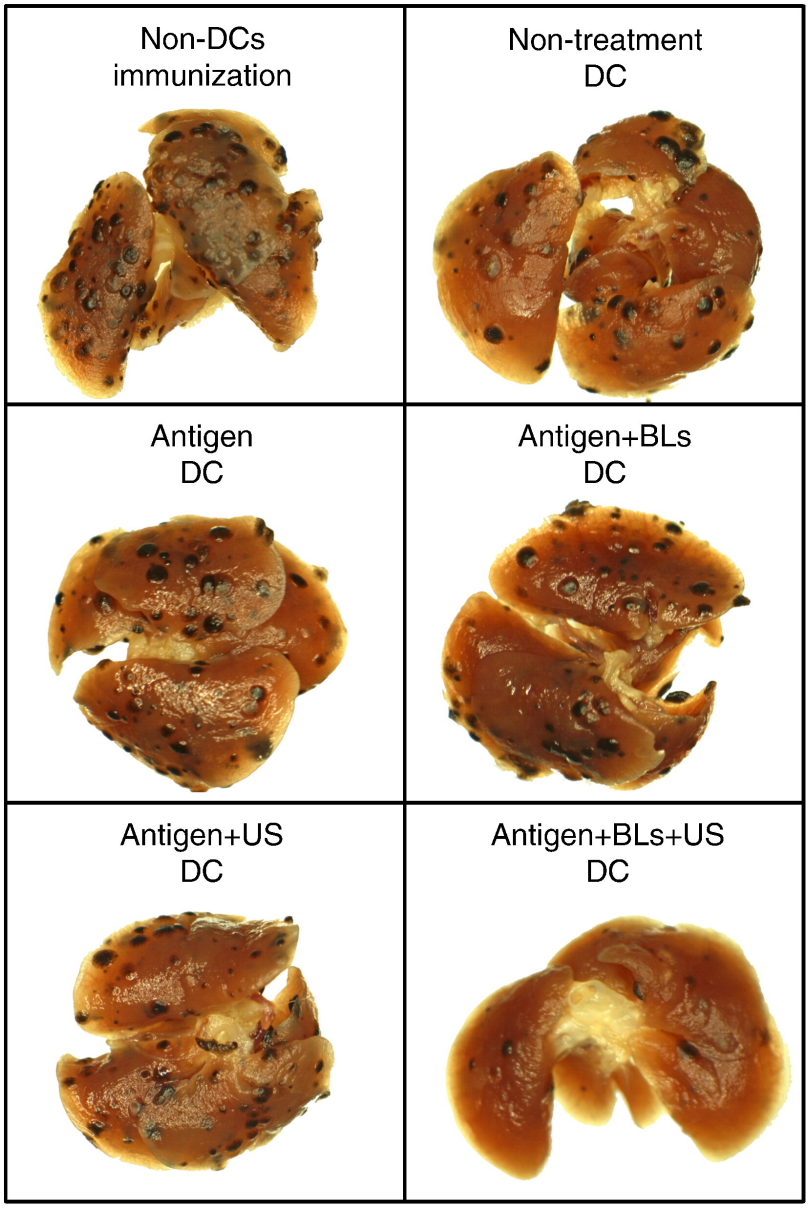
Non-DCs immunization
Non-treatment DC
Antigen DC
Antigen+BLs DC
Antigen+US DC
Antigen+BLs+US DC